INSPYRE
Investigations Supporting MOX Fuel Licensing in ESNII Prototype Reactors

EERA JPNM
JOINT PROGRAMME ON NUCLEAR MATERIALS

D7.3 – Results of the benchmark between pre- and post-INSPYRE code versions on selected experimental cases

B. Boer, J. Eysermans, S. Lemehov (SCK.CEN), L. Luzzi, T. Barani, L. Cognini, A. Magni, D. Pizzocri (POLIMI), A. Del Nevo (ENEA), A. Schubert, P. Van Uffelen (JRC-Karlsruhe), M. Bertolus, M. Lainet, V. Marelle, B. Michel (CEA)

Version 1 – 25/09/2021

The INSPYRE project has received funding from the EURATOM research and training programme 2014-2018 under Grant Agreement No 754329.

Document type	Deliverable
Document number	D7.3 version 1
Document title	Results of the benchmark between pre- and post-INSPYRE code versions on selected experimental cases
Authors	B. Boer, J. Eysermans, S. Lemehov (SCK.CEN), L. Luzzi, T. Barani, L. Cognini, A. Magni, D. Pizzocri (POLIMI), A. Del Nevo (ENEA), A. Schubert, P. Van Uffelen (JRC-Karlsruhe), M. Bertolus, M. Lainet, V. Marelle, B. Michel (CEA)
Release date	25/09/2021
Contributing partners	SCK.CEN, POLIMI, ENEA, JRC-Karlsruhe, CEA
Dissemination level	Public

Version	Short description	Main author	WP leader	Coordinator
1	First release	B. Boer (SCK CEN) 10/08/2021	L. Luzzi (POLIMI) 23/09/2021	M. Bertolus (CEA) 25/09/2021

SUMMARY

This report presents the results of the simulation of the SUPERFACT-1, RAPSODIE-I and NESTOR-3 irradiation experiments using the fuel performance codes TRANSURANUS, MACROS, GERMINAL. The simulations aim at the evaluation of the code improvements made during the INSPYRE project. The comparison of the integral pin performance results with experimental measurements available from the irradiation experiments considered and the comparison between the code results are presented. Both the results obtained using the 'pre-INSPYRE' code versions and the improved 'post-INSPYRE' ones, in which novel data and models originating from other Work Packages of the INSPYRE Project were implemented, are provided.

CONTENT

GLOSSARY

ALFRED	Advanced Lead cooled Fast Reactor European Demonstrator
bfc	bottom of fuel column
DIN	Deutsches Institut für Normung
dpa	displacements per atom
EOL	End Of Life
FGB	Fission Gas Behaviour
FGR	Fission Gas Release
FIMA	Fissions per Initial Metal Atom
FPC	Fuel Performance Code
IAEA	International Atomic Energy Agency
INSPYRE	Investigations Supporting MOX Fuel Licensing for ESNII Prototype Reactors
JOG	Joint Oxyde-Gaine
LWR	Light Water Reactor
MCP	Mid-Core Plane
MOX	Mixed-Oxide
NEA	Nuclear Energy Agency
NRT	Norgett-Robinson-Torrens
PIE	Post-Irradiation Examination
ppn	peak power node
STP	Standard Temperature and Pressure
TD	Theoretical Density
TU	TRANSURANUS fuel performance code

1 INTRODUCTION

1.1 Content of this report

This report presents the results of the simulation of the past fast reactor irradiation experiments SUPERFACT-1, RAPSODIE-I and NESTOR-3 using the GERMINAL, MACROS and TRANSURANUS fuel performance codes. The simulations aim at the evaluation of the code improvements made during the INSPYRE Project. The comparison of the code results with experimental measurements available from the irradiation experiments considered and the comparison between the code results are also presented. The resulting new code versions are referred to as 'post-INSPYRE', while the reference ones as 'pre-INSPYRE'. Note that for readability purposes in all the figures and tables below, the two sets of results are referred to as 'NEW' and 'REF' respectively.

1.2 Code improvements

The new models developed in INSPYRE, their implementation in the GERMINAL, MACROS and TRANSURANUS codes and the corresponding code version numbering are described in detail in Deliverable D7.2 [1]. In summary,

- The GERMINAL and TRANSURANUS codes were improved by integrating:
  - New correlations for MOX fuel thermal conductivity, heat capacity (in GERMINAL) and melting temperature
  - New correlations for MOX fuel thermal expansion and Young's modulus
  - The SCIANTIX inert gas behaviour module, coupled to the FPCs.
- MACROS improvements concern only the implementation of the new correlations for MOX thermal expansion and Young's modulus.

1.3 Evaluation procedure / strategy

The evaluation strategy employed is described in detail in MS15 [2]. The results yielded by the codes involved are compared to the experimental data available, i.e., integral and local post-irradiation examination data. The employed FPCs are also benchmarked by comparing the evolution during irradiation of quantities of engineering interest (fundamental in determining the pin performance).

2 SIMULATION OF THE SUPERFACT-1 EXPERIMENT

2.1 Description of the experiment

Among the irradiation campaigns whose information and experimental results are available to the European fuel performance code (FPC) community, the SUPERFACT-1 irradiation experiment [3] has been selected as part of the INSPYRE FPC assessment strategy, as representative of MOX fuel irradiation in sodium fast reactor environment. Moreover, the minor actinide content (americium and neptunium) in the SUPERFACT-1 pellets allows the analysis of the behaviour of nuclear fuel under fast neutron irradiation for transmutation purposes.

The SUPERFACT-1 irradiation experiment was conducted jointly by CEA, France and ITU, now JRC-Karlsruhe, Germany, between 1984 and 1993 in the Phénix sodium-cooled fast reactor [3]. The detailed

description of the SUPERFACT-1 irradiation experiment is included in INSPYRE Deliverable D7.1 and Milestone MS15 [2].

The goal of the experiment was to investigate how mixed oxide fuel doped with small contents of the minor actinides (MAs) Np and Am behaves under irradiation in a fast spectrum reactor, in order to demonstrate the feasibility of MA transmutation through homogeneous (i.e., low MA content) and heterogeneous (i.e., high MA content) fuel concepts [4]. In the current report, the focus is on the homogeneous concepts, represented by the fuel pins SF7 and SF13, bearing 2 wt.% of ^{237}Np and by the pins SF4 and SF16, bearing 1.8 wt.% of ^{241}Am. The irradiation of the fuel, manufactured at ITU, took place in the Phénix reactor between the 38th and 42nd cycles (October 1986 – January 1988). The maximum linear power reached during the experiment was around 38.7 kW/m, while the peak fuel burnup at the end of life was about 6.5 at.% and the peak cladding damage about 52 NRT-dpa[1]. Post irradiation examinations (PIEs) were performed both at CEA and ITU, covering a wide set of non-destructive and destructive analyses [3]–[5].
The as-fabricated geometry and the characteristics of the considered pins are recalled in Table 1. The fuel pin consists of a stack of solid pellets, all with the same composition and a cladding made of 15-15Ti stabilized, cold-worked austenitic stainless steel. Table 1 also reports the geometric dimensions of the fuel-to-cladding gap, upper and lower plenum [2]. A spring is present in the upper plenum to hold the fuel stack in position during the loading procedures. The sodium coolant conditions and channel properties are reported in [2]. The evolution in time of the linear heat rate is reported in Figure 1.

Table 1: Design parameters of the considered fuel pins from the SUPERFACT-1 experiment.

Parameter	SF7 and SF13	SF4 and SF16
Pellet radius (mm)	2.68	2.71
Radial gap (mm)	0.143	0.116
Pellet density (%TD) [a]	97.5	96.3
Initial grain diameter (µm)	10	10
U/M (wt./) [b]	0.741	0.745
M.A./M (wt./)	0.02, ^{237}Np	0.018, ^{241}Am
Pu/M (wt./) [c]	0.244	0.237
O/M	1.943	1.957
Fuel column mass (g)	207.24	209.61
Fissile column length (mm)	850	
Cladding material	15-15, Ti stabilized, CW SS	
Cladding thickness (mm)	0.45	
Upper plenum volume (mm^3)	1930	
Lower plenum volume (mm^3)	19530	
Helium (filling gas) pressure (MPa)	0.1	
Helium (filling gas) temperature (°C)	20	

[a] Theoretical Densities: 11.077 g/cm^3 for the Np-bearing MOX (pins SF7 and SF13), 11.131 g/cm^3 for the Am-bearing MOX (pins SF4 and SF16)
[b] Natural uranium composition
[c] ^{238}Pu 1.3%, ^{239}Pu 60.4%, ^{240}Pu 23.4%, ^{241}Pu 10.4%, ^{242}Pu 4.5%

After the shutdown, the fuel pins were stored for 1020 days before PIE analyses were performed. The axial power and flux shapes are defined through peak factors, as a result of which the peak power node

[1] The Norgett–Robinson–Torrens displacements per atom (NRT-dpa) model is the current international standard for quantifying the energetic particle damage of the lattice of a material [44].

(ppn) is located slightly below the half of the active fuel column, i.e., at 382.5 mm from the bottom of fuel column (bfc). The complete information about the SUPERFACT-1 irradiation history is collected in[2], based on [3]. The power history of the SUPERFACT-1 experiment is shown in Figure 1.

2.2 Results and discussion

The simulation outcomes concerning the selected fuel pins (SF13 and SF16) from the SUPERFACT-1 irradiation experiment are presented and discussed below. Since the results exhibit very similar trends for the two pins, we show in the figures below only the results on the Np-bearing pin SF13, while the results on the Am-pin SF16 are collected in Appendix A.

The results from each involved code are compared to the available experimental measurements, consisting in both integral and local post-irradiation examination data [3]–[5]. The FPCs employed are also benchmarked by comparing the evolution during irradiation of quantities of engineering interest (fundamental in determining the pin performance).

2.2.1 Time-dependent results

Figure 2 shows the evolution of the fuel centreline temperature of the SF13 Np-pin. Note that in all figures 'pre-INSPYRE' results are referred to as 'REF' and 'post-INSPYRE' results as 'NEW'. As a result of the linear power level of 380 W/cm reached during the reactor start-up at the beginning of life shown in Figure 1, the calculated fuel centreline temperatures are between 2000°C and 2500°C. Significant discrepancies can be noticed in the temperature regimes predicted by the codes, in terms both of values and of dynamics, especially in the early reactor cycles. Discrepancies smooth out towards to end of irradiation. The difference is larger for the SUPERFACT-1 Np-pin, reaching up to five hundred degrees during the second reactor cycle. Generally, TRANSURANUS provides the highest temperature regimes, while GERMINAL the lowest. These discrepancies may be ascribed to the different approaches adopted in the codes to model the fuel radial relocation (stochastic in nature and subject to large uncertainties, based on [6], [7] in TRANSURANUS, while computed through an empirical formulation with fitted parameters in GERMINAL), gap conductance accounting for gap closure, fuel creep and thermal expansion [7]–[9]. Additionally, the fuel central temperature decrease predicted by GERMINAL during the first and the second power cycles is also linked to the increase of the oxygen-to-metal ratio (O/M) into the fuel, due to the consumption of the fissile atoms. Following the reduction in the deviation from stoichiometry of the fuel (initially hypostoichiometric, see Table 1), the thermal conductivity of the material is improved, leading consequently to the temperature decrease in the pellets.

The evolution of the fuel inner radius at the peak power node is shown in Figure 3. Similar dynamics (i.e., fast inner void formation as fuel pins are brought to power) can be recognized in TRANSURANUS and MACROS results, although the asymptotic values predicted by the codes are significantly different. MACROS predicts the formation of the largest central void, consistently with Figure 10. In GERMINAL the inner void size evolution shows a gradual increase along irradiation and is discontinuous due to the discrete finite element mesh used for the computation [9], but it follows correctly the power cycles. A similar stepwise central void behaviour is predicted by MACROS, although much less affected by the various power cycles, as from TRANSURANUS calculations after the first rise to power. These discrepancies between the codes in the prediction of the central hole formation are linked to the different temperature profiles predicted in the fuel pellets: a quicker central hole formation is predicted in relationship with the higher temperature regime in the fuel. In general, a slightly higher inner void size in time is predicted for the Am-pin, with the differences among the code results ascribable to the different densification and restructuring models available in the codes [6], [9]–[13].

As a result of the fuel thermal expansion and restructuring during the first hours and days of the irradiation, the pellet-cladding gap closes, as shown in Figure 4. Again, significant differences arise in

the code calculations, mainly linked to the discrepancies in the predicted temperature regimes (see Figure 2). In particular, MACROS and GERMINAL predict a fast closure of the gap in both considered pins at the beginning of irradiation, ascribed to fuel relocation and fuel creep modelling [9], [13], while TRANSURANUS predictions suggest a slower closure of the fuel-cladding gap, leading to the highest temperature regime predicted in the fuel pellets. According to TRANSURANUS simulations, the gap never closes in both pins at the peak power node, although it almost reaches closure at the end of irradiation. In addition, the effect of gap re-opening when power drops is more pronounced in TRANSURANUS and MACROS. It is important to underline that, in addition to beginning-of-life phenomena (fuel and cladding sudden thermal expansion, fuel relocation and restructuring), other irradiation phenomena contribute to determine the gap dynamics, such as fuel swelling, cladding creep and swelling. In particular, the differential swelling of fuel and cladding along irradiation is lower in TRANSURANUS calculations than in GERMINAL and MACROS predictions.

The cladding outer diameter change increases as a result of the thermal expansion, although some permanent deformation can be identified due to radiation-induced swelling (and creep), as seen in Figure 5. The values reached at the beginning of life (just after the first rise to power) are different among code predictions (although slightly different), suggesting a possible difference in the linear thermal expansion coefficients considered by the codes [8], [9], [13], [14]. The cladding outer temperature at the beginning of life is the lowest from TRANSURANUS calculations (around 500°C), while slightly higher according to GERMINAL and more than 10°C higher according to MACROS, consistent with a higher cladding thermal expansion after the first power ramp. Moreover, while TRANSURANUS and GERMINAL predict consistent (with the power evolution) and similar trends for both the SUPERFACT-1 pins, MACROS results show a stronger effect of the power variations, leading to the highest cladding outer radius values. The cladding geometry is affected by fuel-cladding contact and hence by fuel swelling, as well as by cladding creep and swelling. The latter two phenomena are particularly delicate to model and depend significantly on the empirical correlations included in the codes. In particular, TRANSURANUS relies on a correlation predicting the onset of cladding swelling [8], while the GERMINAL swelling model comes into play when a threshold incubation dose for swelling to occur is reached at the considered axial position [9].

Figure 6 shows the increase of the gap internal pressure with irradiation time induced by the fission gas production and release shown in Figure 7. The three codes all predict a similar release fraction of 55-65% for end-of-life conditions. Both quantities are largely determined by the temperature regime experienced by the fuel column during irradiation. Hence, the differences among the codes' predictions of the fuel temperature are reflected in these calculations. A significantly different dynamics of fission gas release, characterized by a fast increase up to ~ 60% during the first reactor cycle (Np-bearing pin), then following the power cycles up to an end-of-irradiation value of ~ 65%, is predicted by TRANSURANUS with respect to GERMINAL and MACROS (see Figure 7). The trends of fission gas release predicted by GERMINAL and MACROS also show a pronounced impact of the fourth power cycle, which corresponds to the maximum linear power of the entire irradiation history. In TRANSURANUS, fission gas release is computed using a model featuring a threshold for the grain face fractional coverage above which the inter-granular gas release happens [15]. In GERMINAL on the contrary, the fission gas release is computed using an empirical formulation where the temperature effect is introduced through a thermal activation term [9]. The decrease of the GERMINAL prediction during the third cycle of irradiation, visible also in the TRANSURANUS result, is therefore caused by the lower operating power during this cycle. The pressures in the fuel-cladding gap (Figure 6) yielded by the three codes for both SUPERFACT-1 pins are consistent with the evolution of the fission gas release, both in values and in trends.

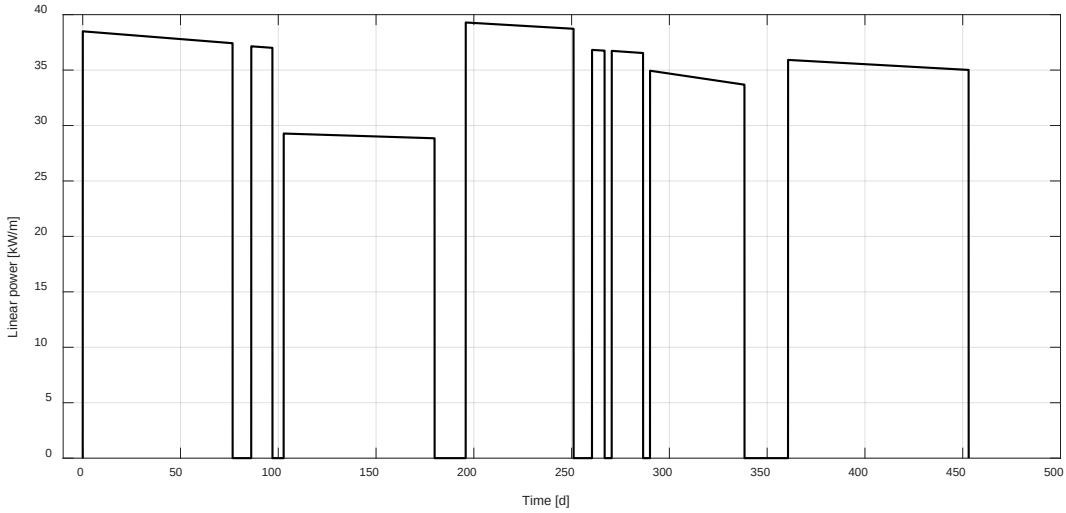

Figure 1: Power history of the SUPERFACT-1 experiment for SF13 fuel pin at the peak power node [3].

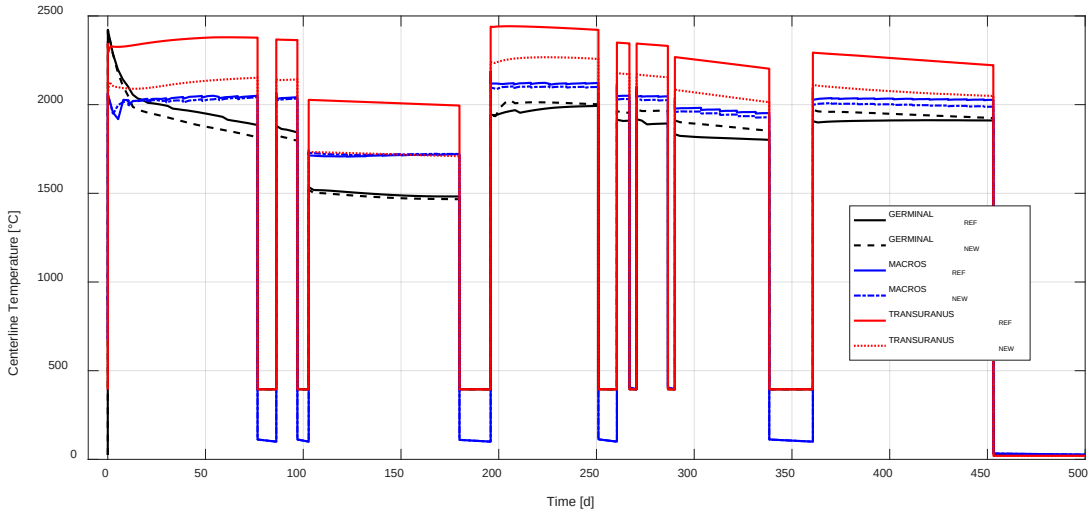

Figure 2: Fuel centreline temperature evolution during the SUPERFACT-1 experiment for SF13 fuel pin at the peak power node.

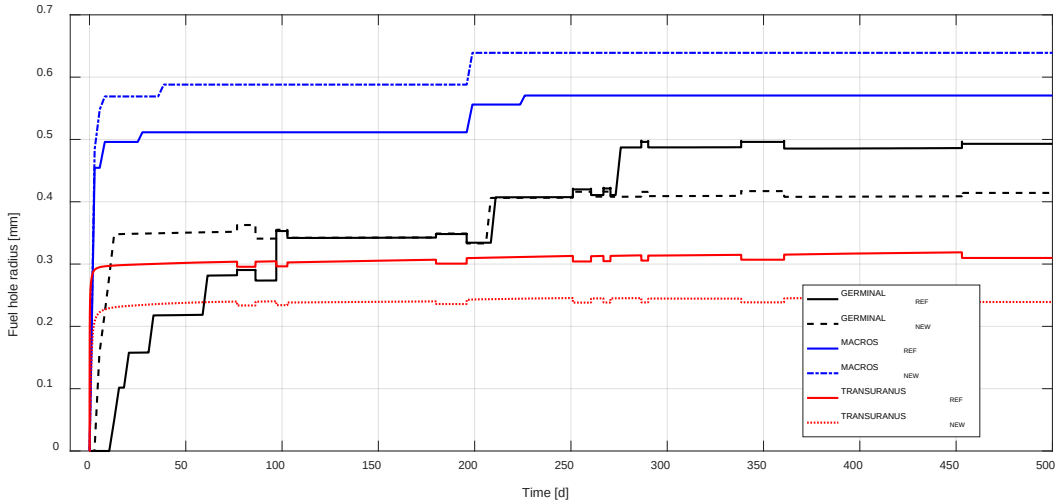

Figure 3: Fuel inner radius (hole) evolution during the SUPERFACT-1 experiment for SF13 fuel pin at the peak power node.

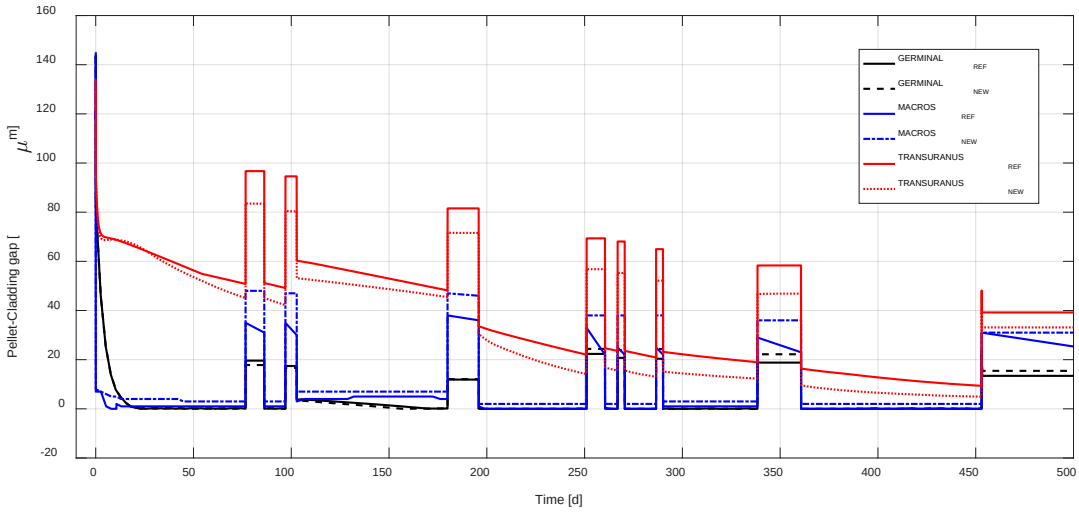

Figure 4: Fuel-cladding gap evolution during the SUPERFACT-1 experiment for SF13 fuel pin at peak power node.

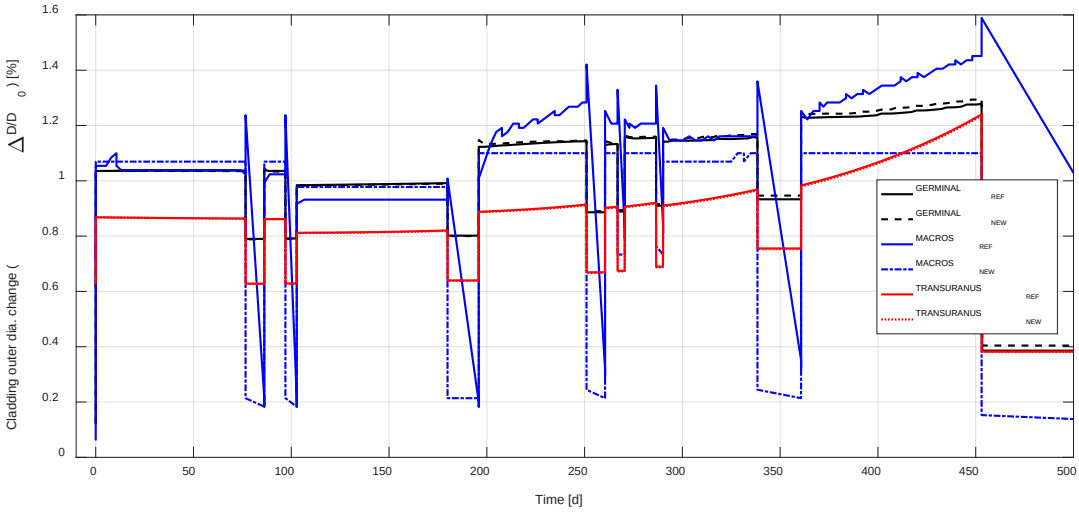

Figure 5: Cladding outer diameter change evolution during the SUPERFACT-1 experiment for SF13 fuel pin at peak power node.

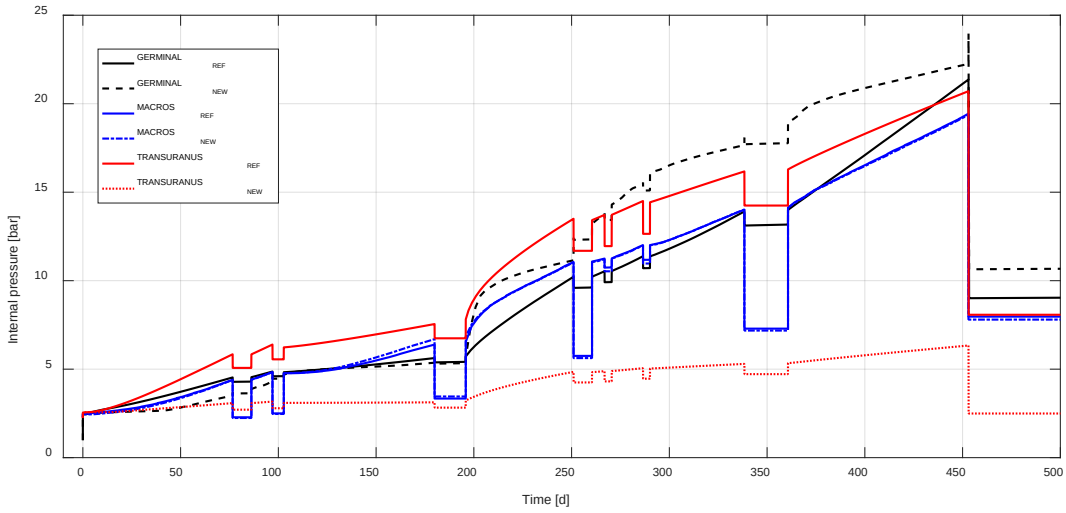

Figure 6: Internal gas pressure evolution in the fuel-cladding gap during the SUPERFACT-1 experiment for SF13 fuel pin at peak power node.

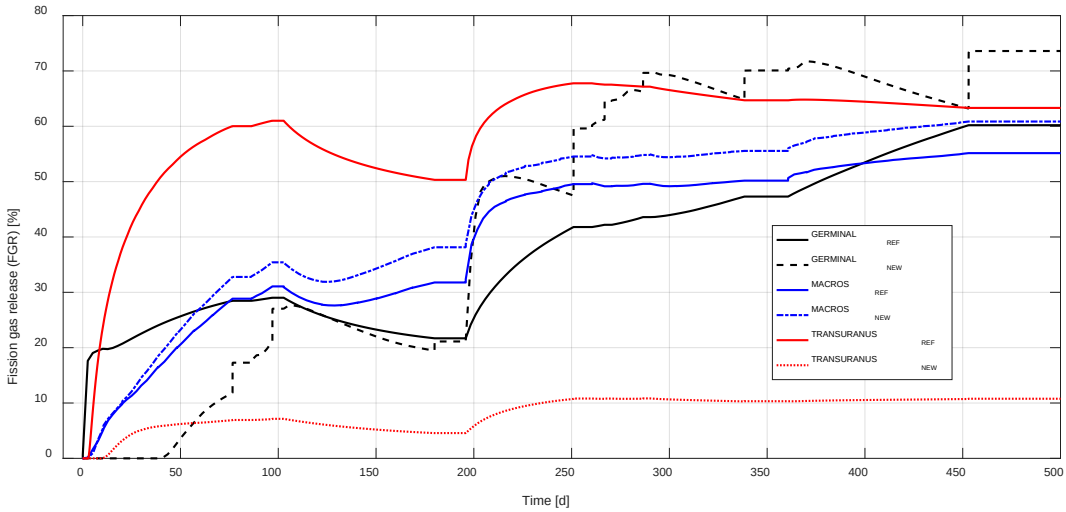

Figure 7: Fission gas release during the SUPERFACT-1 experiment for SF13 fuel pin.

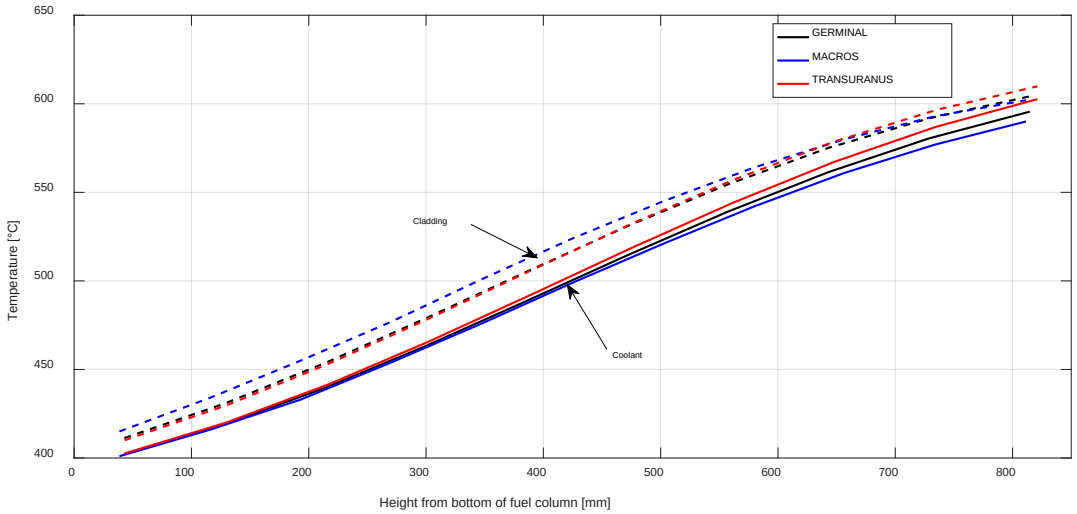

Figure 8: Cladding and coolant temperature axial profiles after 1 hour of operation during the SUPERFACT-1 experiment for SF13fuel pin. Only the pre-INSPYRE code versions are shown for sake of clarity of the plot since there are no significant variations using post-INSPYRE code versions.

The main differences as follows can be identified between the results of the pre- and post-INSPYRE code versions:

- The post-INSPYRE TRANSURANUS version yields a significantly lower fuel centreline temperature as compared to the pre-INSPYRE one. This affects the fuel restructuring, leading for instance to a smaller fuel central void evolving during irradiation (Figure 3). More importantly, a much lower release fraction of fission gases and consequently a lower inner pin pressure is predicted because of the coupling with the SCIANTIX module. This module is equipped with physics-based and FBR-tailored models but requires a coherent TRANSURANUS-SCIANTIX framework for the proper simulation of FBR conditions (in particular a fuel grain growth model suitable for fast reactor fuel and conditions).
- The post-INSPYRE GERMINAL version yields a faster formation of the central hole, which is more in line with the predictions of the two other codes.

No major difference can be found between the pre- and post-INSPYRE results of the MACROS code. Only a wider fuel inner void and a more stable and consistent evolution of the cladding outer diameter are observed, as can be seen in Figure 3 and Figure 5, respectively.

2.2.2 Radial and axial profiles and comparison with experimental data

The axial and radial profiles of the cladding deformation, the extent of fuel restructuring (central void and columnar grain zone) and the concentrations of important element (Np, Pu, Xe and Cs) are reported and compared with measured data in the figures below.

The comparison of calculated outer cladding diameter at the end of life (including the storage time before PIEs) for the SF13 fuel pin with the experimental clad profilometry is reported in Figure 9.

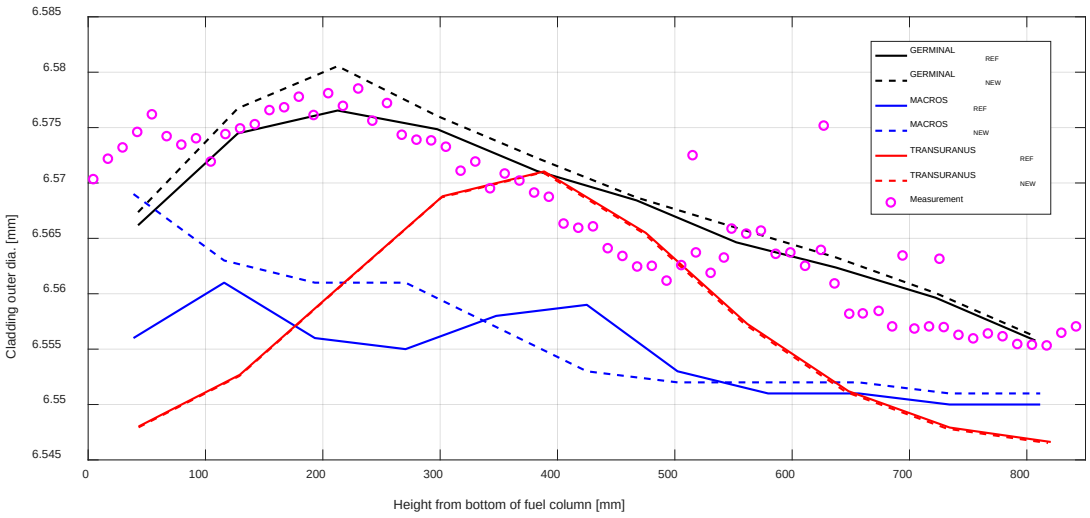

Figure 9: Axial profile of cladding outer diameter of the SUPERFACT-1 pin SF13 at peak power node.

The overall agreement of the simulation results using the pre-INSPYRE code versions with the experimental measurements is satisfactory. The agreement of GERMINAL predictions with data from the Np-pin is excellent thanks to its refined cladding swelling model based on the large experimental database available at CEA [9]. Some small differences between the Am (see Appendix A) and the Np fuel pins can be observed in the cladding diametrical deformation yielded by TRANSURANUS and MACROS, whereas no differences are observed in the GERMINAL results. These different trends between codes are mainly explained by the fact that the GERMINAL computation is based on the initial diameters measured of the fuel pins (6.555 and 6.554 mm, respectively) while TRANSURANUS/MACROS results are based on initial diameters given in Table 1 (6.552 mm for the Am fuel pin and 6.546 mm for the Np fuel pin). The minor differences among the code results can have three origins: the different empirical correlations employed to calculate the cladding swelling rate, the temperature and dose thresholds triggering the swelling and the different correlations employed to compute cladding creep. Both irradiation-induced and thermal creep are considered by the codes: TRANSURANUS solves the constitutive equations for the non-linear mechanical behaviour, including the creep and swelling treatment, in an additive formulation of inelastic strains [8], [16]. GERMINAL uses a similar approach but employs different creep and swelling correlations [9]. The different treatments of fuel creep and swelling can partially explain the discrepancies seen in the cladding profilometry predictions, especially where fuel-cladding closure takes place. Gap closure is predicted at the peak power node by GERMINAL and MACROS, as shown in Figure 9. The maximum cladding diameter measured experimentally, however, is located below the peak power node, where the temperature is deemed too low to activate a recovery process able to reduce the swelling rate despite a higher dose at the peak power node. This effect is well represented by GERMINAL, while TRANSURANUS predictions are largely determined by the axial shape of the linear power and fast neutron flux, suggesting a predominant impact of irradiation swelling and creep on the predicted cladding profilometry at the end of life. The different dependencies on the irradiation damage of the correlations employed by the codes for cladding swelling and creep prove to be the main cause of discrepancies in the code calculations shown in Figure 9. The cladding profilometry results are impacted by the level of fuel-cladding mechanical interaction in case of gap

closure, which is predicted by GERMINAL and MACROS. The MACROS results show a general under-estimation of the experimental profilometries.

In Figure 10 and Figure 11, we compare the axial profiles of fuel inner diameter and columnar grain diameter at the end of life, respectively, yielded by the codes and the experimental data on fuel restructuring. TRANSURANUS predictions of the inner void diameter are remarkable, as can be seen in Figure 10, but reveal clearly different profiles compared to GERMINAL and MACROS axial results. The central void formation in TRANSURANUS and GERMINAL is computed from a multi-physics formulation coupling thermo-mechanical aspects and fuel restructuring through a vaporization-condensation process and porosity migration and involving specific model parameter fitting [9], [8]. The restructuring model in MACROS, accounting for the coupled formation of columnar grains and central void, adopts a semi-empirical approach linking the local radial temperatures with the characteristic restructuring propagation time. The MACROS model features an activation energy associated with vaporization/ sublimation processes and a minimal temperature required for the onset of fuel restructuring. This temperature is set to 1800°C, consistently with experimental observations [13], [17].

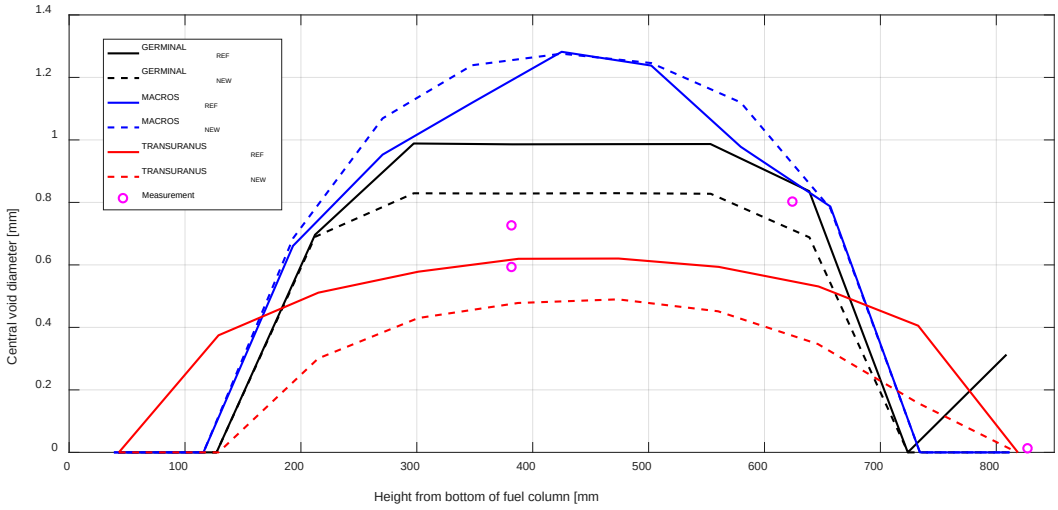

Figure 10: Axial profile of central void diameter of the SUPERFACT-1 pin SF13 at peak power node.

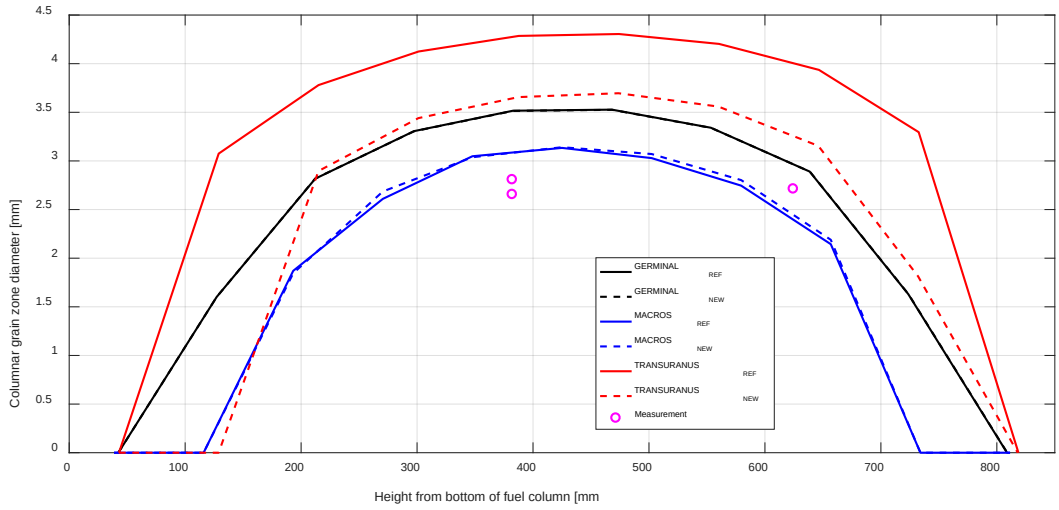

Figure 11: Axial profile of the diameter of the columnar grain zone of the SUPERFACT-1 SF13 pin at the peak power node.

TRANSURANUS overestimates the axial extent of the inner void, which is probably linked to an over-prediction of the fuel central temperature, but correctly predicts the observed absence of a central void

at the top of the fuel column at the end of life. This overestimation is also indicated by the predictions on the diameter of the columnar grain region reported in Figure 11. TRANSURANUS tends to over-estimate the extension of this region, implying an overestimation of the fuel temperature regime. On the contrary, the agreement of GERMINAL and MACROS results on the extension of columnar grains with the experimental data is good, despite the over-estimation of the inner void size at the end of life. Then, fuel restructuring is absent at the active fuel column extremities according to both GERMINAL and MACROS simulation results. GERMINAL predicts an unusual opening of the fuel central void at the top of the fuel column in the Np-bearing pin, linked to a local overestimation of the fuel temperature due to an overestimation of the gap size. This suggests the need for improvements concerning the modelling of the central hole formation, the fuel restructuring and the pellet-cladding gap closure coupled effects, as well as a better formulation of the relocation model (see reference [18]). It is worth noting that the inner void diameter final value may be affected not only by the fuel restructuring, which usually takes place at the beginning of irradiation, but also by fuel inward creep, which can occur if fuel-cladding contact is established.

The calculated radial profiles of plutonium concentration at the peak power node are compared with the experimental data in Figure 12. A remarkable agreement of the TRANSURANUS results with the measurements can be observed. GERMINAL also provides a satisfactory agreement at the pellet periphery. These codes predict a substantial redistribution of plutonium across the pellet, consistent with PIE results. This effect is, however, somewhat overestimated by GERMINAL, i.e., a stronger migration of plutonium from the intermediate pellet radii to the inner pellet region is obtained. The models employed by GERMINAL and TRANSURANUS, considered as the best-estimate ones for fast reactor MOX fuel in the state-of-the-art FPCs, rely on several parameters and include dependencies on local quantities impacting on the performance results (e.g., oxygen-to-metal ratio (O/M), above all) [9], [19]. The models are still subject to revisions and improvements. For O/M ratios corresponding to slightly hypostoichiometric fuel (O/M between 1.97 and 2.00), the partial vapour pressures of U and Pu oxides are similar, so there is not a preferential redistribution of one element on the other [20]–[22]. The lack of sensitivity to the O/M ratio represents a current limitation of the redistribution process modelling and calls for a comprehensive thermo-chemical modelling of the fuel under irradiation [9], [23], in combination with dedicated experiments and atomic scale simulations (e.g., [24]). On the contrary, as shown by Figure 12, the MACROS code does not currently include a redistribution model.

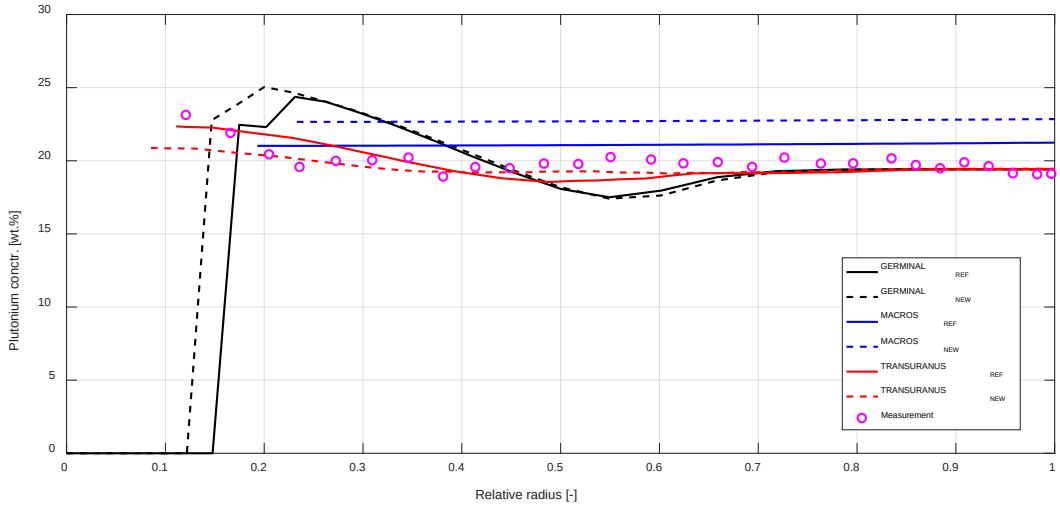

Figure 12: Radial profile of the plutonium concentration of the SUPERFACT-1 pin SF13 at the peak power node.

The predictions of neptunium radial concentration at the peak power node are compared to experimental data in Figure 13. Under fast reactor conditions, americium is subject to redistribution

either due to solid-state diffusion or evaporation-condensation mechanisms, because of the steep radial temperature gradient and high temperature levels. Neptunium is considered to be less or not affected by redistribution mechanisms [25]–[27]. The TRANSURANUS model for actinide redistribution therefore considers only plutonium and americium redistribution [26], whereas the evolution of the neptunium radial concentration during irradiation is only determined by fuel burnup. The GERMINAL code includes also a model for neptunium redistribution [9]. The flat MACROS results are consistent with the fact that its burnup model is not yet coupled to an actinide redistribution model [13]. The overall agreement of the code predictions is good for both neptunium and americium, considering the experimental uncertainties [4], [5]. The accuracy of GERMINAL calculations is remarkable, although showing a concentration step close to the central void, due to an artefact which allows moving from the finite volume mesh (used to solve the porosity migration equation) to the finite element mesh of the multi-physics formulation. TRANSURANUS overestimates the radial redistribution of americium (see Appendix A, Figure 59) and the average concentrations of Am and Np at the end of life, which could point to a need for revision of some cross-sections of the code database.

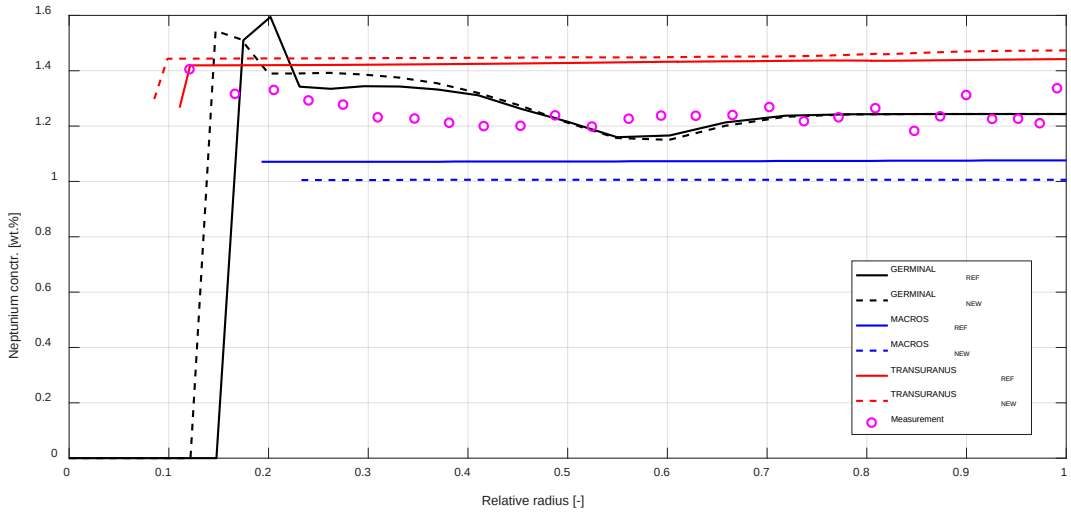

Figure 13: Radial profile of the Np concentration of the SUPERFACT-1 SF13 pin at peak power node.

The comparisons of measured against predicted xenon and caesium radial concentration are presented in Figure 14 and Figure 15. The Xe concentration is well caught by MACROS and TRANSURANUS in the inner and outer regions of the pellet, while some discrepancies arise at intermediate radii. This result indicates that these two codes do not describe correctly the onset of fission gas release in the SUPERFACT-1 fuels. In GERMINAL calculations, the increase of Xe concentration at the pellet periphery is linked to a threshold temperature for the gas release, i.e., the intra-granular diffusion coefficient features a thermal activation term [9]. Only MACROS displays the same Xe concentration radial profiles for the Am and the Np bearing pins, with concentrations lower than the experimental ones at inner and intermediate radii. As for caesium, the code predictions are based on a simplified description of its production, evolution and release by fuel grains. For example, in TRANSURANUS and GERMINAL the caesium release is correlated to the xenon one [8], [9] and the models do not account for the various possible compounds caesium can form or the various possible phases, liquid, vapour or gaseous, depending on local temperature and oxygen potential. Hence, the current models do not include the various mechanisms of Cs axial migration and underestimate the experimental concentrations measured in the outermost region of the pellet. The MACROS code predicts the increase in the concentration of Cs retained in the fuel grains at higher radii than observed experimentally. This causes a significant underestimation of the measured caesium profiles in the intermediate pellet region, which is the most challenging region for the code simulations. It is worth pointing out that the concentrations of fission gases and other fission products retained in the outer region of the fuel pellets and their release in the fuel-cladding gap are also influenced by the formation and evolution of the High Burnup Structure

(HBS). This a fuel microstructure evolution towards smaller grains and elevated porosity occurrs at sufficiently high burnup and temperatures lower than 1000°C [28]–[30]. The effect of HBS on the fission gas behaviour mainly consists in the depletion of fission gases from the fuel matrix and accumulation in the HBS pores. The final peak burnup reached by the SUPERFACT-1 fuels considered here (~ 65 GWd/t) suggests the absence or a limited formation of the HBS, experimentally observed to start at local burnups between 60 and 75 GWd/t and still under investigation [31], [32].

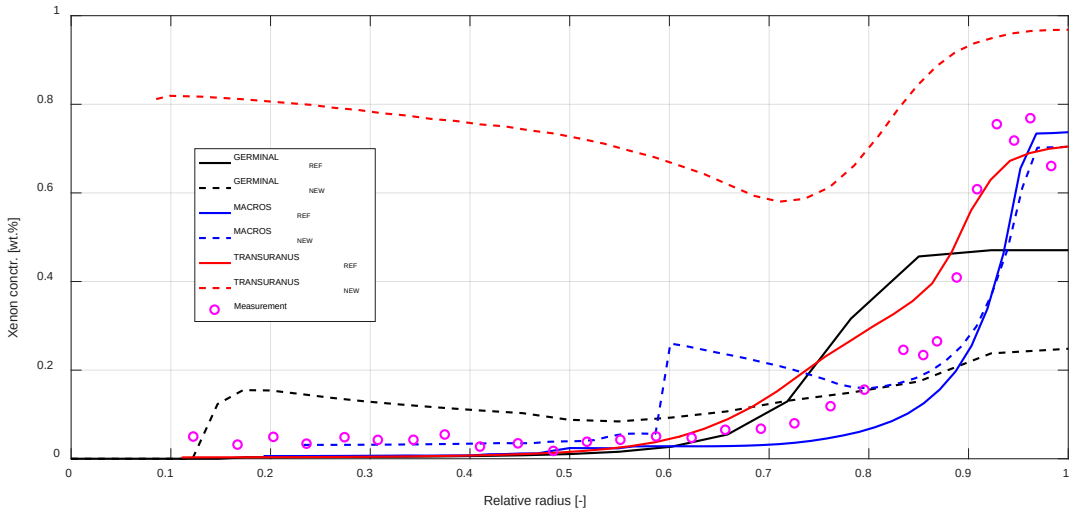

Figure 14: Radial profile of the Xe concentration of the SUPERFACT-1 SF13 pin at peak power node.

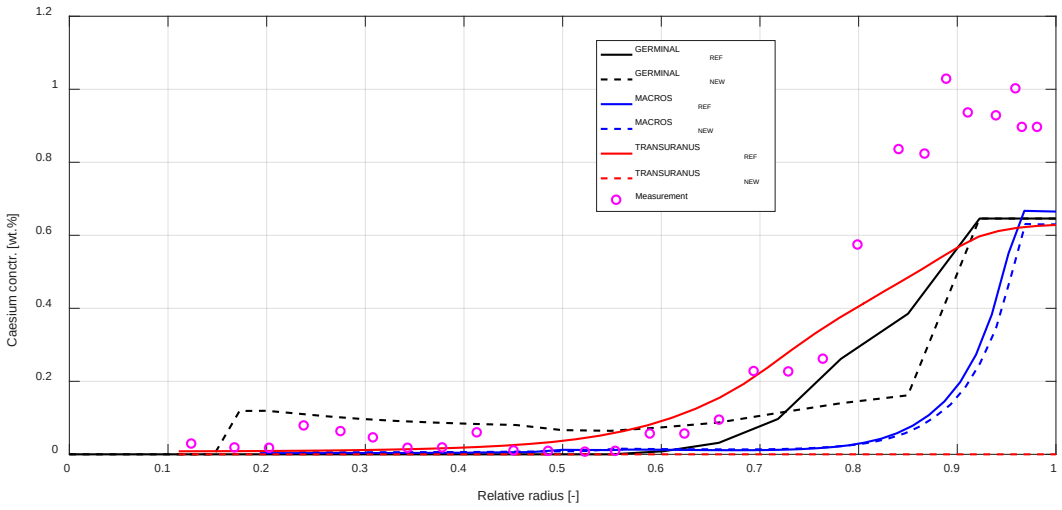

Figure 15: Radial profile of the Cs concentration of the SUPERFACT-1 SF13 pin at peak power node.

The use of the post-INSPYRE versions of the GERMINAL and TRANSURANUS codes yields a smaller central void, while the effect is opposite but less evident for MACROS. Moreover, TRANSURANUS predicts a smaller columnar grain region, i.e., a consistently reduced fuel restructuring resulting from the lower fuel temperatures (Figure 2). The results of the post-INSPYRE version of TRANSURANUS also exhibit substantial differences in the Xe and Cs radial concentrations. This is partly due to the lower temperatures obtained, but mostly to the application of the SCIANTIX module for fission gas behaviour and release, which yields a much higher Xe retention in the fuel pellets. The latter seems more compatible with LWR conditions for which the SCIANTIX module was originally developed, and mainly ascribable to the TRANSURANUS grain growth model, which is currently tailored on LWR fuels and irradiation conditions. The Cs behaviour is not yet described in SCIANTIX, resulting in a null radial concentration for this element. Finally, there are no major difference between the results of the pre- and post-INSPYRE MACROS and GERMINAL code versions concerning the Xe and Cs concentrations.

2.2.3 Integral code results and comparison with experimental data

As already mentioned in the previous sections, the most noticeable difference between pre- and post-INSPYRE results is related to the TRANSURANUS-SCIANTIX coupled simulation, which shows a much smaller FGR (10% compared to 55%) and a smaller void length (closer to the experimental measurement). In Section 2.3 below, further sensitivity studies are performed with TRANSURANUS, in order to investigate the impact of the different INSPYRE models alone on the results from the extended code. The updated MACROS results show a lower fuel elongation and a larger void length as compared to the original results. Instead, the integral results from the updated GERMINAL code are mostly coincident with the reference ones, apart from a higher fission gas release at the end of life (74% instead of 60%).

In particular, the TRANSURANUS pre-INSPYRE version overestimates the axial extent of the fuel central hole in both fuel pins considered. This can be ascribed to an overall overestimation of the temperature regime along the fuel column. Moreover, the fuel column elongation yielded by the various codes do not compare well with the experimental data. They are strongly overestimated by TRANSURANUS and MACROS pre-INSPYRE versions, while they are underestimated by the pre and post-INSPYRE versions of GERMINAL. A correct estimation of fuel elongation remains difficult, considering the complexity of the mechanisms involved in the elongation process, which is also influenced by fuel axial relocation and by the constrained boundary conditions induced by the pellet-cladding gap closure. Another difficulty for the assessment is linked to the uncertainty on the fuel column elongation measurements, as the free parts of the fuel stack may move when the fuel pin is handled during the post-irradiation examination.

The amounts of released gas (Xe, Kr, He) measured were obtained from puncturing the rods and sublimation was then applied to measure the gas amounts retained [3]. In order to derive the fractional release, the total gas produced was calculated and is therefore determined indirectly from measurements. The agreement with this volume of fission gases produced is good, while the integral fission gas release is generally underestimated by the three codes. Concerning the estimated volumes of helium release, TRANSURANUS predictions are in reasonable agreement, MACROS results show a close agreement with the experimental value, while GERMINAL prediction is slightly overestimated because of the assumption of total release made.

As already mentioned in the previous sections, the most noticeable difference between the results of pre- and post-INSPYRE is related to the TRANSURANUS-SCIANTIX coupling, which results in a much smaller FGR (10% compared to 55%) and a smaller void length, closer to the experimental measurement. The post-INSPYRE MACROS version yields a lower fuel elongation and a larger void length compared to the pre-INSPYRE one. On the contrary, the integral results yielded by the post-INSPYRE GERMINAL code are mostly similar with those of the pre-INSPYRE version, the only difference being a higher fission gas release at the end of life (74% instead of 60%), closer to the measured FGR of 67%.

Table 2: Comparison between the results of the pre and post-INSPYRE code versions and experimental measurements [3] for fuel pin SF13 (X: not calculated). For the meaning of 'TU THERMAL', 'TU MECHANICAL' and 'TU SCIANTIX', see the Section 2.3 below.

	Measured	TU REF	TU THERMAL	TU MECHANICAL	TU SCIANTIX	TU NEW	GERMINAL REF	GERMINAL NEW	MACROS REF	MACROS NEW
Final burnup at ppn (at.%)	6.4	6.5	6.5	6.4	6.5	6.4	6.6	6.6	6.8	6.4
Fission gas (Xe + Kr) produced (cm^3)	227*	231	231	227	293	240	228	228	237	225
Fission gas release (%)	67	55	54	52	9	10	60	74	55	61
Kr / (Kr + Xe) (%)	6.9	7.1	7.1	7.1	X	X	7.2	7.1	7.0	13.4
He released (cm^3)	14.2	8.6	8.6	7.6	X	X	22.0	22.0	7.2	3.1
Central hole length (mm)	624 - 643	776	778	777	775	603	426	427	541	618
Fuel elongation (mm)	9.5 – 10.2	25	26	24	20	21	2	2	39	18
Clad elongation (mm)	1.60	1.4	1.4	1.4	1.4	1.4	-0.1	-0.1	1.6	0.8

*Calculated value from experimental information.

2.3 Sensitivity studies

A sensitivity study was performed on the TRANSURANUS results in order to assess in detail the impact of each model developed in the INSPYRE Project. The code extensions as follows were analysed separately on the SUPERFACT-1 Np-pin SF13:

- The improved MOX thermal properties – results referred to as 'TU THERMAL';
- The improved MOX mechanical properties – results referred to as 'TU MECHANICAL';
- The incorporation of the SCIANTIX module for fission gas behaviour and release modelling – results referred to as 'TU SCIANTIX'.

In addition, fast reactor fuel performance can be impacted by the formation of a Joint Oxyde-Gaine (JOG), the additional oxide layer thought to be primarily composed of caesium molybdate (Cs_2MoO_4) that fills the fuel-cladding gap at high burnup under certain temperature conditions. The effect of the JOG formation and evolution in the fuel-cladding gap was assessed using the GERMINAL code, which is the only code involved in the Project that includes a model of the JOG effects on the pin performance.

For the assessment of the various TRANSURANUS code versions, we focus on the fuel central temperature, fuel-cladding gap size, fractional fission gas release and fuel central hole size at the peak power node as a function of time.

It can be seen in Figure 16 that the largest impact on the central temperature evolution comes from the novel thermal conductivity correlation for MOX fuels described in D7.2 [1] and [33] and included in TU THERMAL. The post-INSPYRE description of the thermal properties also results in the formation of a smaller central hole due to the lower temperature regime (see Figure 19), but still occurring very quickly at the beginning of irradiation, as expected. The lower fuel central temperature is also reflected in the larger gap size due to the reduced thermal expansion and consequently also in the reduced fission gas release at the beginning of irradiation.

Following the strong rise in power at 200 days of irradiation, however, there is a larger increase of the fission gas release due to the accumulated (and not yet released) amount of fission gases. Because of the higher fission gas release and the open gap situation, the gap conductance is affected and leads to reduced differences in the fuel central temperature between on the one hand the TU-THERMAL and TU-NEW (post-INSPYRE) code versions and on the other hand the TU-REF (pre-INSPYRE) version towards the end of irradiation (Figure 16).

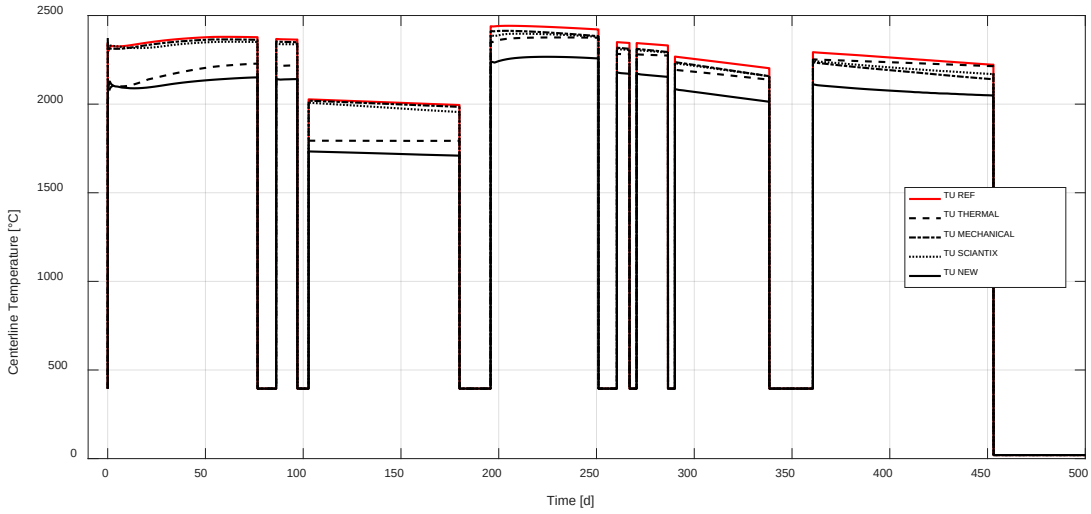

Figure 16: Evolution of the fuel centreline temperature for the SUPERFACT-1 SF13 pin at the peak power node, for several TRANSURANUS modelling assumptions.

The effect of the modified mechanical properties (thermal expansion coefficient and Young's modulus) can be analysed by comparing the curves obtained using the pre-INSPYRE TRANSURANUS version and TU MECHANICAL for the pellet-cladding gap (Figure 17). Unsurprisingly, the impact is most pronounced on the gap size. More precisely, the gap between the pellets and the cladding is smaller, leading to lower temperatures (Figure 16). This effect is smaller than expected because of the compensating reduced thermal expansion of the pellets. This underlines the non-linear character of the pellet behaviour that is impacted both by the thermal and mechanical properties simultaneously.

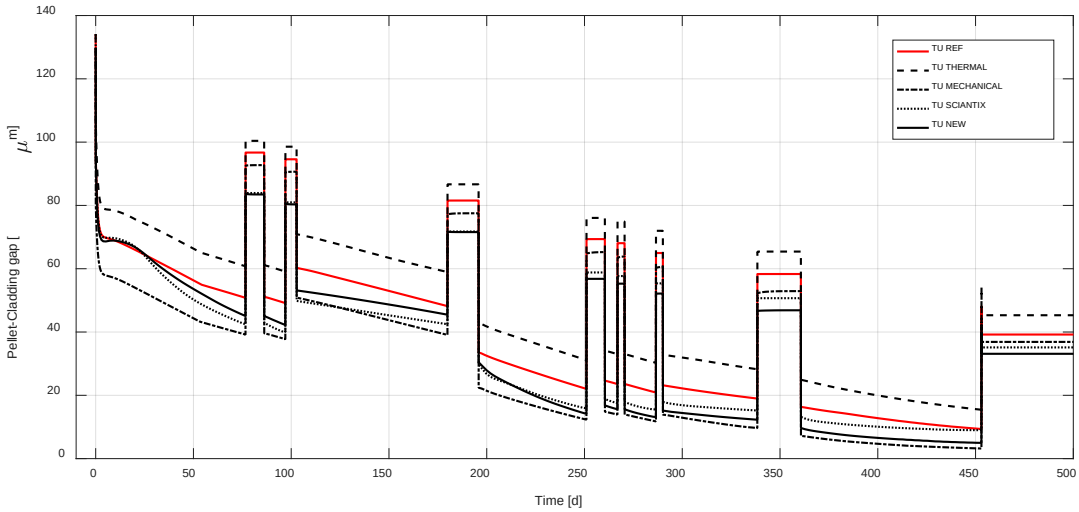

Figure 17: Evolution of the pellet-cladding gap for the SUPERFACT-1 SF13 pin at the peak power node, for several TRANSURANUS modelling assumptions.

The impact of employing the mechanistic fission gas behaviour SCIANTIX module instead of the standard fission gas behaviour model available in TRANSURANUS is clearly seen in the evolution of the integral fractional fission gas release (
Figure 18). An example of development needed to improve the simulation of FBR irradiation conditions is the update of the grain growth model impacting the grain boundary bubble behaviour [34] to account properly for the temperature ranges typical of FBR fuels. A similar impact was observed when integrating the SCIANTIX code in the GERMINAL code, but the issue was solved by limiting the fuel grain growth. This update is included in the post-INSPYRE GERMINAL version.

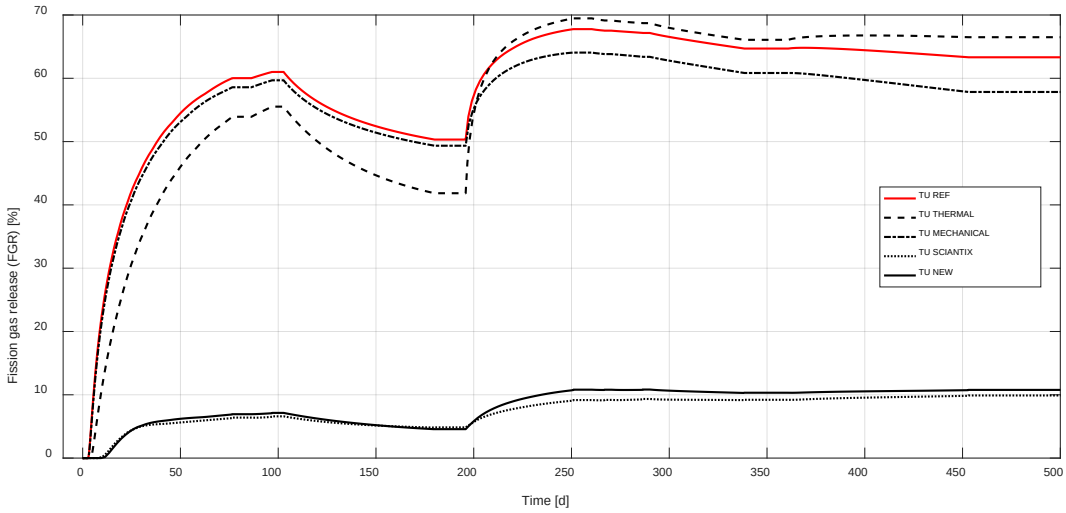

Figure 18: Evolution of the FGR for the SUPERFACT-1 SF13 pin at the peak power node, for several TRANSURANUS modelling assumptions.

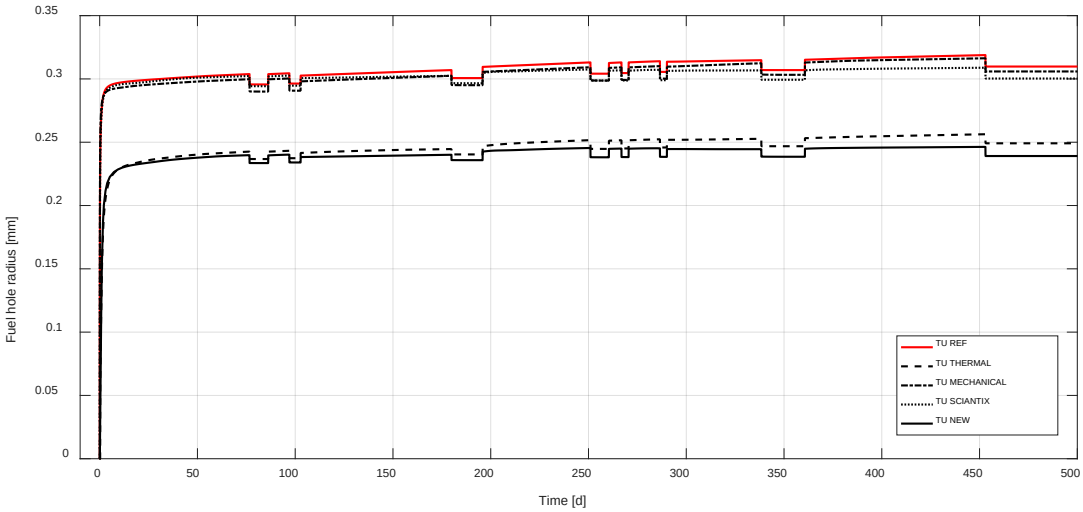

Figure 19: Evolution of the central void formation of the SUPERFACT-1 SF13 pin at the peak power node, for several TRANSURANUS modelling assumptions.

In general, the fast reactor fuel performance is impacted by the formation of the JOG, which can currently be modelled using the GERMINAL code. The final fuel burnup reached in the SUPERFACT-1 experiment, however, is lower than the threshold value after which the JOG formation is observed experimentally in the database used for the JOG modelling in GERMINAL [9] and no impact is expected.

2.4 Conclusions on the SUPERFACT-1 simulation results

The simulation of the SUPERFACT-1 SF13 and SF16 pins proves that the results of the three fuel performance codes considered exhibit an encouraging agreement with the available experimental data. Substantial room for improvements, however, emerges from this work. Code development paths can be identified and were partly addressed within the INSPYRE Project:

- Fuel relocation at beginning of life: Given the stochastic nature and large impact of this phenomenon, this would help to harmonize the spread in centreline temperature predictions arising from our calculations, especially at the beginning of life.
- Gap conductance: A deeper analysis of the gap conductance models applied in the various codes based on separate-effect experimental data could also contribute to the reduction of the spread in temperatures observed at the beginning of the irradiation.
- Behaviour and redistribution of volatile fission products: The comparisons between experimental and calculation results point out a substantial deviation (e.g., on radial caesium concentration, likely due a currently incorrect / unsatisfactory description of volatile fission products transport and behaviour in mixed oxide fuels).
- Behaviour of fission gases: The comparisons concerning the radial distribution of xenon, the integral quantity of fission gas (xenon and krypton) and helium released call for a step forward on the modelling. In particular, adapting fully the SCIANTIX module to fast breeder reactor conditions and harmonizing its coupling with TRANSURANUS seems recommended.
- Fuel mechanical behaviour: The substantial differences between the results of the various codes concerning the gap evolution under irradiation – besides the aforementioned relocation on the fuel side – call for a more accurate description of temperature-driven phenomena (e.g., fuel thermal creep) which would eventually influence the gap dynamics.

Further code developments would also be needed on the behaviour of the stainless-steel cladding under irradiation in sodium fast reactor conditions. In particular, the comparisons of calculated and experimental cladding profilometries show substantial differences between the results of the three

codes. This is likely due to the different correlations and models implemented in the codes to account for cladding creep and void swelling. The improvement of these models is out of the scope of INSPYRE, which focuses on the fuel itself. It is the subject of the ongoing H2020 European Projects GEMMA and Il Trovatore. This part of code improvement would benefit from the exchange of information between EU projects.

3 SIMULATION OF THE RAPSODIE-I EXPERIMENT

3.1 Description of the experiment

The RAPSODIE-I (also named SNR 1) experiment was performed in the framework of the SNR-300 reactor research program in the Rapsodie sodium fast reactor, between 1971 and 1972. It contained two fuel assemblies of 34 pins each with MOX fuel of two different suppliers (Alkem and Belgonucleaire) and two different cladding materials (DIN 1.4988 and DIN 1.4970). Both attained a peak burnup level of about 10% FIMA and a peak cladding damage of about 35 dpa_{NRT} [35]. Only the DIN 1.4970 pins were considered in the INSPYRE code assessment. The geometry and characteristics of the AU-01 and BU-14 fuel pins are provided in Table 3.

Table 3: Design parameters of the considered AU-01 and BU-14 fuel pins from the RAPSODIE-I experiment [2].

Parameter	AU-01*	BU-14*
Pellet radius (mm)	2.56	2.53
Radial gap (mm)	0.065	0.099
Pellet density (%TD)	87.0	86.9
Initial grain diameter (µm)	12	12
U[a]/M	0.70	0.70
M.A./M	0	0
Pu[b]/M	0.30	0.30
O/M	1.990	1.965
Fissile column length (mm)	320	320
Cladding material	DIN 1.4970, CW + A	
Cladding thickness (mm)	0.361	0.376
Ar + He (filling gases) pressure [c] (MPa)	0.1	0.1
Upper plenum volume[d] (mm^3)	844	849
Lower plenum volume[d] (mm^3)	4741	4766
[a] ^{235}U/U 83% in wt		
[b] ^{238}Pu 0.016%, ^{239}Pu 89.99%, ^{240}Pu 9.12%, ^{241}Pu 0.817%, ^{242}Pu 0.057% in wt.%		
[c] 10.4% Ar and 89.6% He		
[d] Gross plenum volume not taking into account spring or other internal structures.		

* AU = Alkem, BU = Belgonucleaire. For the Alkem pellet density the value from Ref. [36] is adopted here and considered the correct one. According to Table II on page 2 of Ref. [35], the bulk density of the Alkem (AU) fuel pellets is between 83.6 and 85.2% TD.

The details about the axial nodalization needed for the simulation of the fuel pins, together with the peak factors needed to obtain the axial shape of the linear heat rate and fast neutron flux (different between the beginning of life, BOL and the end of life, EOL), are collected in [2]. The power histories experienced by the AU-01 and BU-14 pins are shown in Figure 20.

3.2 Results and discussion

The RAPSODIE-1 irradiation experiment was simulated using the pre- and post-INSPYRE versions of the TRANSURANUS and MACROS codes.

3.2.1 Time-dependent results

The results of the simulations of pin AU-01 are shown in the figures below: evolution of the fuel centreline temperature in Figure 21, fuel inner radius in Figure 22, pellet-cladding gap size in Figure 23, cladding outer diameter change in Figure 24, internal gas pressure in Figure 25 and fission gas release in Figure 26. The simulation results of the BU-14 pin, which are not reported here, show trends similar to the AU-01 ones. Axial profiles at EOL and integral results concerning the AU-01 pin are given in Sections 3.2.2 and 3.2.3, respectively.

The simulations yield the results as follows:

- As a result of the relatively high linear power up to 490 W/cm (see Figure 20), the fuel centreline temperature calculated varies between 2350°C and 2500°C depending on code / version (Figure 21).
- As a result of the high temperature, a significant fuel central hole forms, with a radius between 0.6 mm and 0.8 mm (Figure 22).
- The predicted fission gas release is also high, > 60% after ~ 50 days as can be observed in Figure 26, except for the post-INSPYRE version of the TRANSURANUS code when coupled with the SCIANTIX FGB module, as for the SUPERFACT-1 case (see Section 2.3).
- As a result of the fission gas release, the pin internal pressure increases with increasing fuel burnup level, as shown by Figure 25, although it remains low for post-INSPYRE TRANSURANUS due to the low FGR predicted.
- The pellet-cladding gap closes during the irradiation with progressive burnup, but both codes predict the gap re-opening at the cold state at EOL (Figure 23). This effect is more evident from MACROS calculation than from TRANSURANUS, together with a different dynamics of the gap size evolution along the pin irradiation.

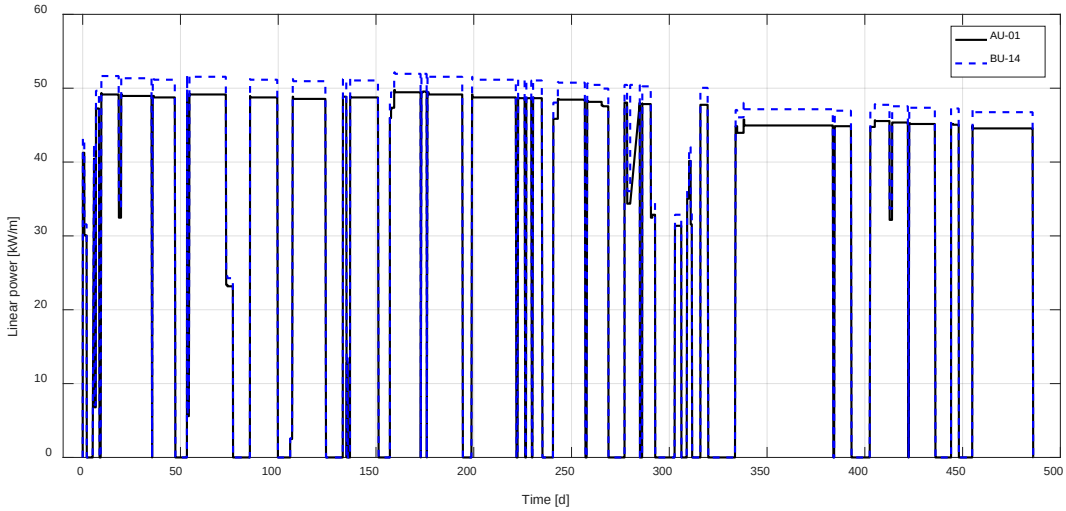

Figure 20: Power histories of the RAPSODIE-I AU-01 and BU-14 fuel pins at peak power node.

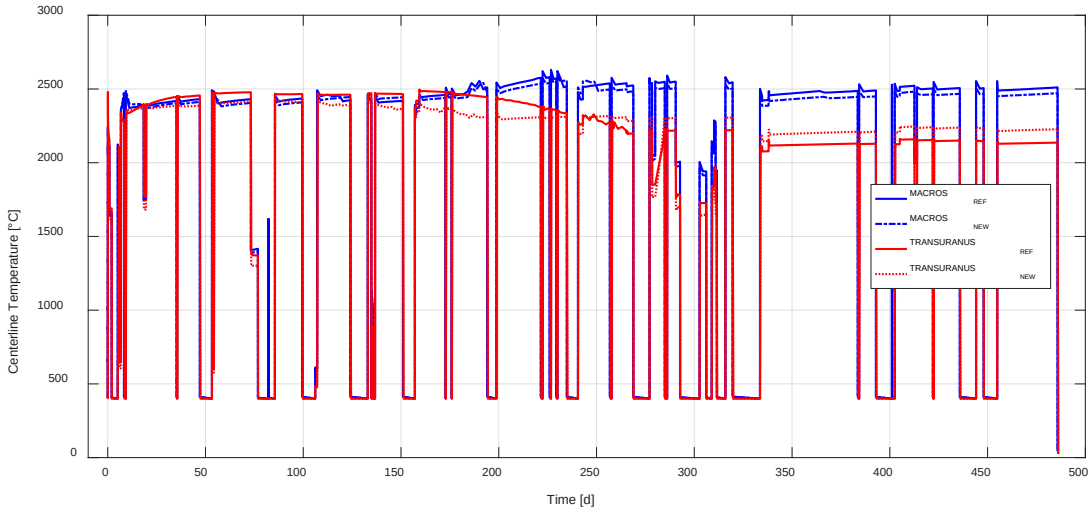

Figure 21: Fuel centreline temperature evolution of the RAPSODIE-I AU-01 pin at peak power node.

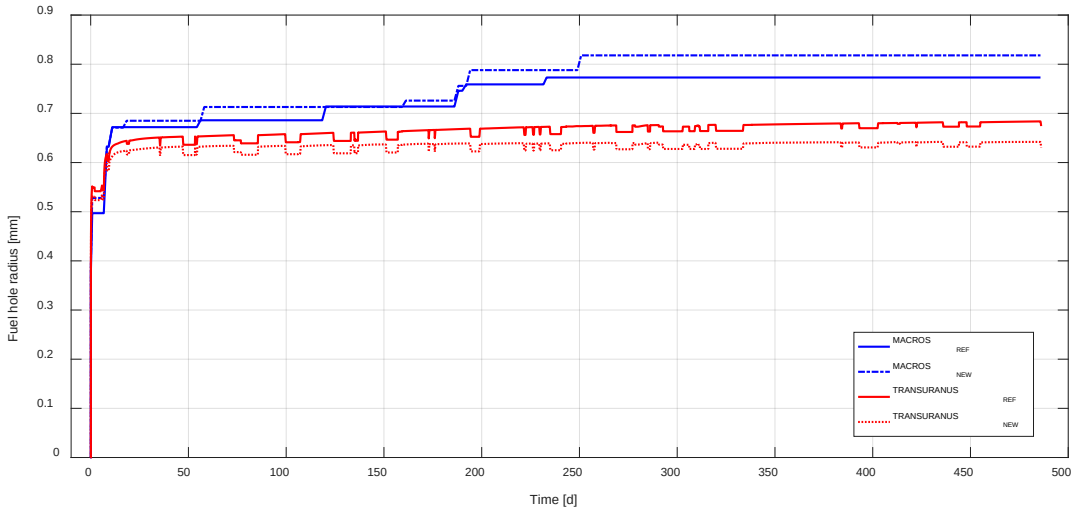

Figure 22: Inner fuel radius (hole) evolution of RAPSODIE-I AU-01 pin at peak power node.

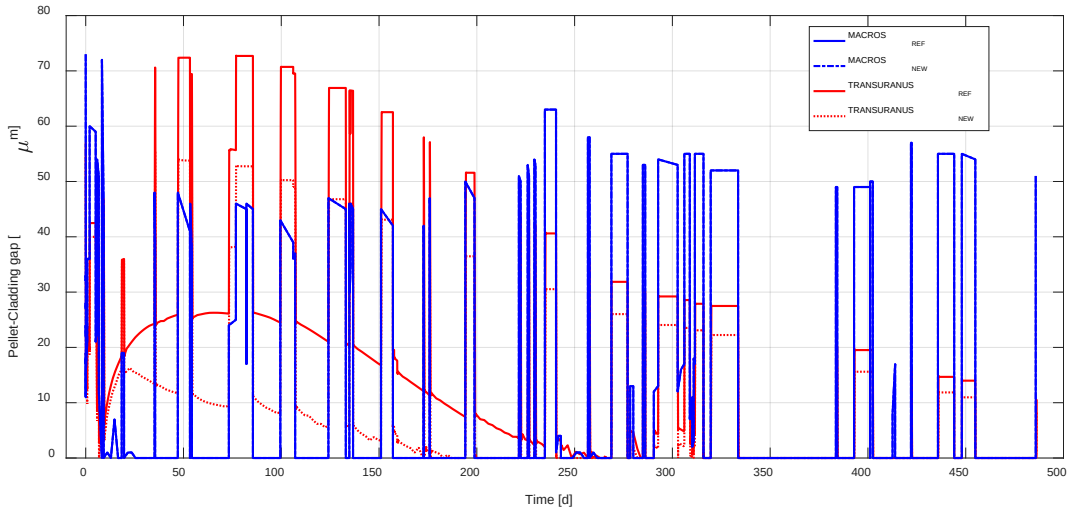

Figure 23: Fuel-cladding gap evolution of the RAPSODIE-I AU-01 pin at peak power node.

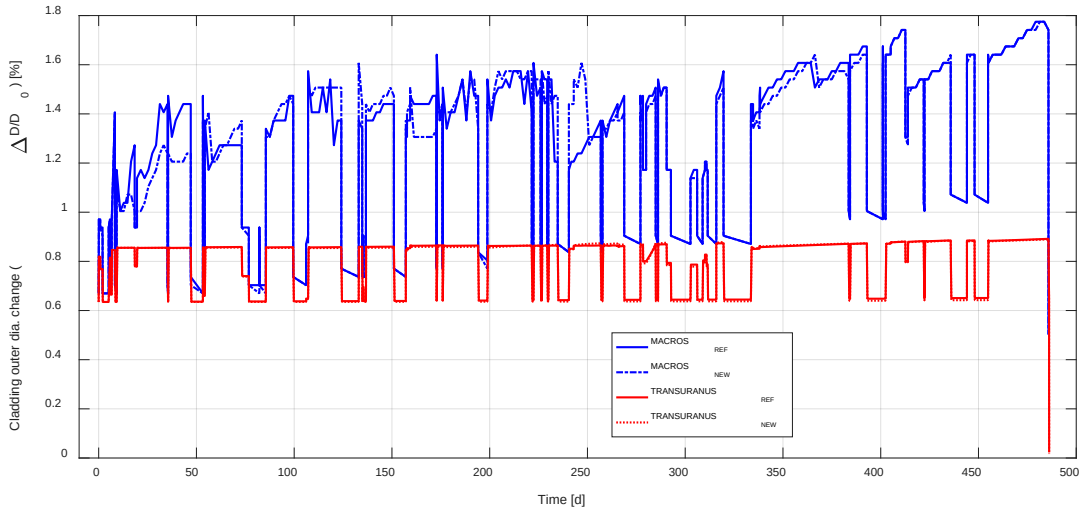

Figure 24: Cladding diameter change evolution of the RAPSODIE-I AU-01 pin at peak power node.

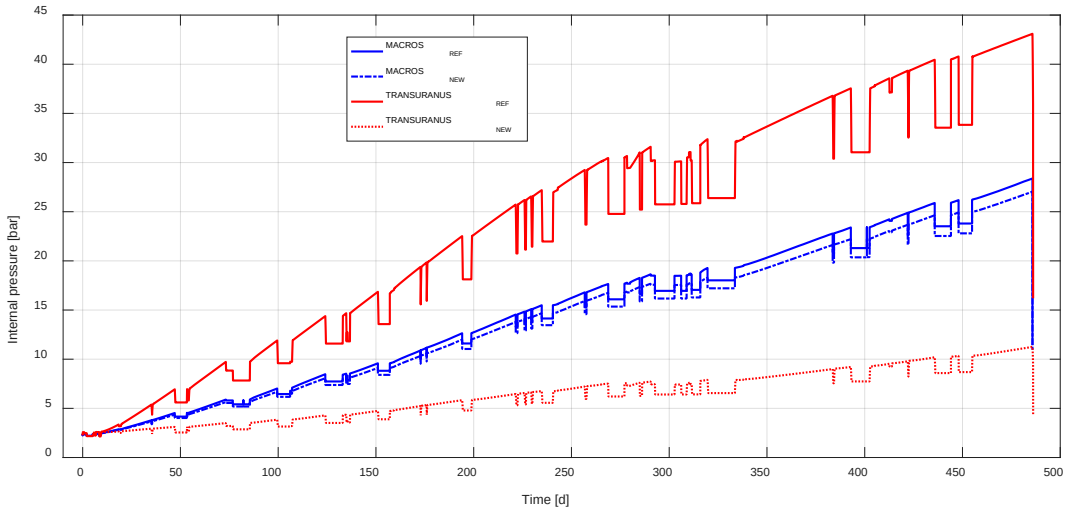

Figure 25: Internal gas pressure evolution of the RAPSODIE-I AU-01 pin at the peak power node.

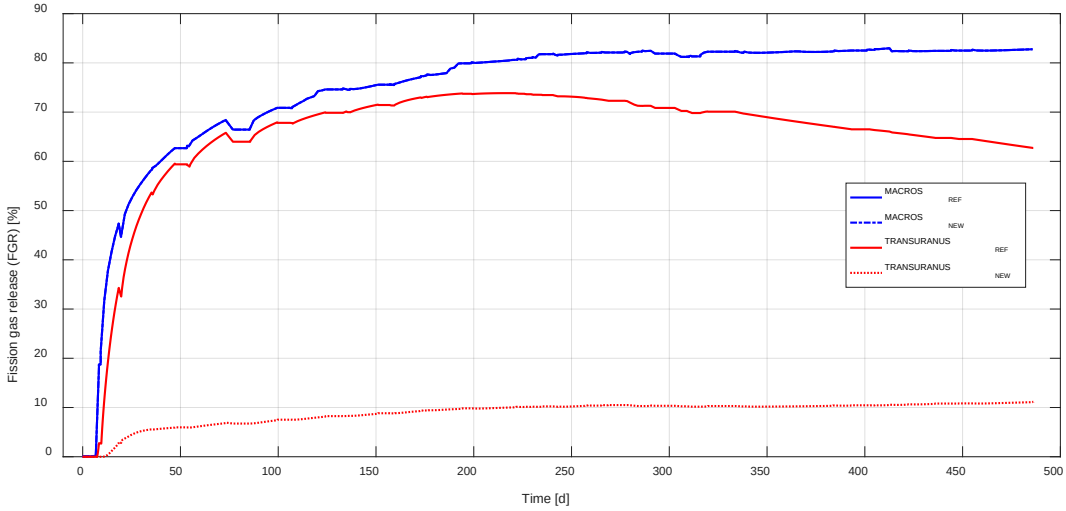

Figure 26: Fission gas release during RAPSODIE-I experiment for AU-01 fuel pin at peak power node.

3.2.2 Axial profiles and comparison with experimental data

The fuel central void diameter and columnar grain zone diameter of pin AU-01 are compared with the measurements in Figure 27 and Figure 28. The sizes of the columnar grain zone and of the fuel central void yielded by the pre- and post-INSPYRE versions of MACROS and TRANSURANUS are in good agreement with the measurements although MACROS post-INSPYRE version predicts no fuel restructuring at the bottom of fuel column.

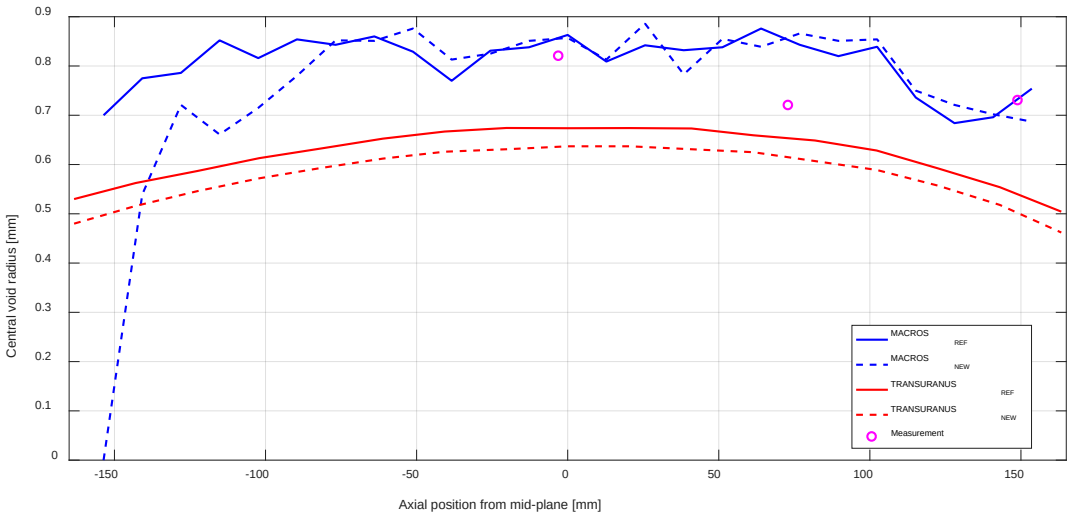

Figure 27. Central void radius at the EOL of the RAPSODIE-I experiment for fuel pin AU-01.

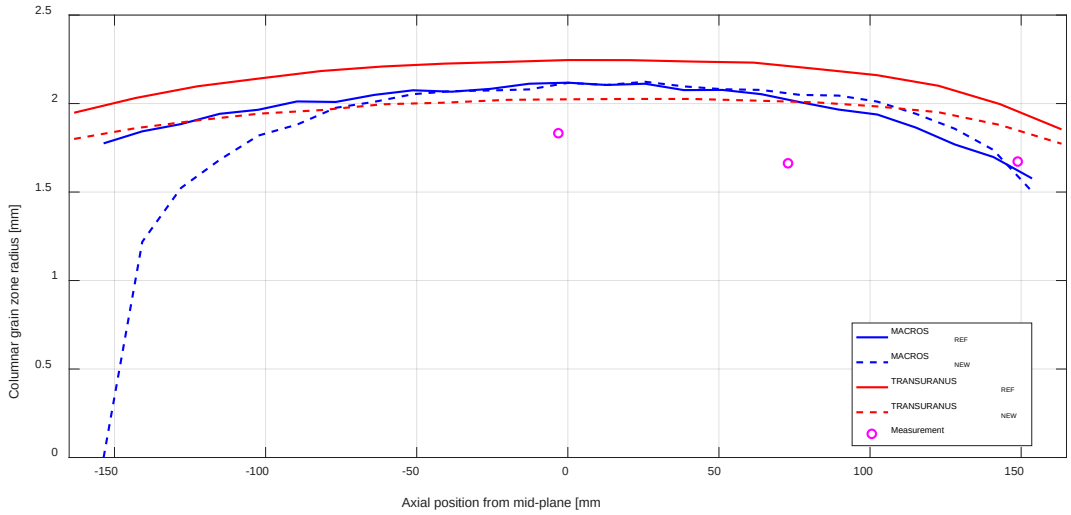

Figure 28: Columnar grain zone radius at the EOL of the RAPSODIE-I experiment for fuel pin AU-01.

3.2.3 Integral code results and comparison with experimental data

The integral results of the simulation of the RAPSODIE-I experiment by the various code versions for the AU-01 and BU-14 pins are compared with the measurements in Table 4 and Table 5, respectively.

It is noted in reference [37] related to the amount of fission gas measured originally at Gfk (now JRC-Karlsruhe), that "some systematic error was made during the puncture tests performed and the (earlier reported) values will not be considered…". Other references [36] of that time appeared to have used the original reported values [35], although it was found later that these values led to FGR fractions above 1. A corrected gas volume was obtained by taking the originally measured puncture data and multiplying them with a correction factor. This factor is calculated as follows: average measured volume of 15 pins

performed at SCK.CEN / average measured volume of 9 pins at Gfk = 1.76 cm^3/g oxide / 2.05 cm^3/g oxide = 0.86. The average oxide mass is 61 g [37].

It can be seen from Table 4 and Table 5 that the agreement with the total volume of fission gas released measured at Standard Temperature and Pressure (STP) is reasonable, especially considering the experimental uncertainty. MACROS provides higher simulated values than TRANSURANUS. The coupling of SCIANTIX with TRANSURANUS, part of the post-INSPYRE strategy, confirms the need of further extensions of its models of fission gas behaviour for FBR conditions. This has already been done for the coupling of SCIANTIX with the GERMINAL code, as discussed in Section 2, in order to account for the fact that the SCIANTIX module was originally developed for LWR fuels and conditions.

Moreover, predictions of fuel elongation do not compare well with the experimental data, in both calculated values and sign. Calculations yield an elongation of the AU-01 fuel pin, while the measurements show a shortening, and an overestimation of the elongation of the BU-14 pin. The PIE reports [35],[37] on the RAPSODIE-I experiment, which contain data for more than just the AU-01 and BU-14 pins, however, show an opposite elongation behaviour among the same pin batch, some pins exhibiting a shortening and other ones an elongation. The data of the 20 pins reported exhibit an average change of the fuel column of +0.03 mm, with a standard deviation of 2.35 mm. Only the MACROS code predicts a shortening of the BU-14 pin, ascribable to fuel restructuring. A correct estimation of fuel elongation remains difficult, considering the complexity of the mechanisms involved in the fuel elongation process.

3.3 Conclusions on the RAPSODIE-I results

The RAPSODIE-I irradiation experiment provides data on fuel pin behaviour in high-power fast reactor conditions. The available data include phenomena that are complex and difficult to model, such as the formation of the fuel central hole, a large columnar grain zone and pellet-cladding interaction at high fuel temperature that is affected by the formation of the JOG, which is not yet modelled by the codes (MACROS, TRANSURANUS) applied in this benchmark exercise. The comparison of the MACROS and TRANSURANUS simulation results yields the main outcomes as follows:

- The estimation of the size of the central void and of the columnar grain region is relatively accurate compared to the available experimental data and consistent between the two codes.
- The estimates of the cladding elongation reveal room for improvement in both codes applied and call for the implementation of a model for the JOG formation and evolution, as well as for the revision of some model parameters, e.g., fuel and clad swelling.
- Fission gas release levels are reasonably estimated by the codes, except for the TRANSURANUS code versions coupled with the SCIANTIX module ('TU SCIANTIX' and 'TU new'), which relies on a model tailored for LWR-fuel grain growth and under extension to fast reactor fuel conditions.

Table 4: Comparison of experimental data and simulation results of integral quantities regarding the AU-01 fuel pin. For the meaning of 'TU THERMAL', 'TU MECHANICAL' and 'TU SCIANTIX', see Section 2.3.

	Measured	TU REF	TU THERMAL	TU MECHANICAL	TU SCIANTIX	TU NEW	MACROS REF	MACROS NEW
Fission gas (Xe+Kr) released STP (cm^3)	94 (104)*	79.0	77.8	95.4	18.1	17.0	100.9	101
Fission gas release (%)	75% (82%)*	62.7	61.6	77.4	11.8	11.0	82.9	82.9
Active fuel column length changes (mm)	-4.3	+13.4	+13.3	+10.4	+13.0	+13.2	+1.25	+1.27

* Originally reported value, see [36].

Table 5: Comparison of experimental data and simulation results of integral quantities regarding the BU-14 fuel pin. For the meaning of 'TU THERMAL', 'TU MECHANICAL' and 'TU SCIANTIX', see Section 2.3.

	Measured	TU REF	TU THERMAL	TU MECHANICAL	TU SCIANTIX	TU NEW	MACROS REF	MACROS NEW
Fission gas (Xe+Kr) released STP (cm^3)	100 (116)*	91.4	90.7	104.3	22.6	22.1	112	113.3
Fission gas release (%)	75% (87%)*	68.8	68.3	80.4	13.9	13.6	82.6	82.56
Active fuel column length changes (mm)	+4.1	+13.8	13.7	12.2	12.6	12.8	-0.93	-0.80

* Originally reported value, see [36].

4 SIMULATION OF THE NESTOR-3 EXPERIMENT

4.1 Description of the experiment

The NESTOR-3 irradiation experiment was performed between 1984 and 1987 on a standard PHENIX fuel assembly made of 217 pins. The peak burnup at the end of life was 13.28 at.% and the benchmark data come from the same fuel pin number 110, except for the fission gas release, extracted from another fuel pin. These two pins were located close to the centre of the assembly (first row and second row). The peak cladding damage at the end of life is greater than 100 dpa_{NRT} [2].

4.1.1 Fuel pin characteristics

The fuel column is composed by fertile pellets at the bottom, surmounted by a longer fissile column. As-fabricated fertile pellets are hollow and made of UO_2, while the material of the full fissile pellets is MOX with a Pu/metal ratio of 22.43%. The cladding material is an austenitic stainless steel. The specifications of the NESTOR-3 fuel pins are given in Table 6, [2].

Table 6: Design parameters of the NESTOR-3 fuel pin, [2].

Parameter	Fissile pellet
External Pellet radius (mm)	2.719
Radial gap (mm)	0.106
Pellet density (%TD)	94.72
U/M	0.78
Pu/M	0.288
O/M	1.975
Column length (mm)	853.5
Cladding material	Austenitic stainless steel 15-15 Ti

4.1.2 Power history

The mean linear power of the NESTOR3 fuel pin at peak power node is equal to 25.7 kW/m.

4.2 Results and discussion

4.2.1 Time-dependent results

The code results on the evolution of the fuel centreline temperature, the pellet-cladding gap evolution, the relative cladding outer diameter change, the fission gas release, the inner pin pressure and the fuel central hole radius are shown in Figure 29 to Figure 34. The Y-axis values of the figures showing the experimental results are not shown to protect the confidentiality of these results.

The trends as follows can be identified from the simulation results:

- The fuel central temperature evolutions obtained (see Figure 29) are consistent with the variation of the power level during the NESTOR-3 experiment, but sensibly different between the various versions of the codes involved, depending mostly on the different thermal conductivity and gap conductance correlations employed. In particular, the decrease in temperature predicted by GERMINAL after approximately 420 days of irradiation is linked to the gap re-opening (Figure 30) due to JOG formation, improving the fuel-cladding gap conductance.

- Because of the high power reached at the beginning of irradiation, a central hole is rapidly formed in the fuel pellet during the first days (Figure 34). However, the codes predict a very different kinetics of the fuel central void evolution. MACROS and GERMINAL seem to follow more closely the power/temperature variations at the start of irradiation. On the contrary, TRANSURANUS predicts a fast void formation during the first rise to power, while the subsequent kinetics is only weakly dependent on the power level.
- The pellet-cladding gap closes progressively with irradiation time (Figure 30). The closure dynamics varies with the code version. GERMINAL predicts a fast gap closure, followed by a sudden re-opening due to JOG formation. After that, the gap size evolution follows the JOG thickness evolution. The gap size according to TRANSURANUS and MACROS is subjected to a slower closure and after its re-opening (controlled by fuel and cladding differential swelling and thermal expansions), TRANSURANUS leads to the highest EOL value, while MACROS to the lowest one. In particular, TRANSURANUS predicts a strong cladding swelling due to radiation damage towards the EOL due to the neutron fluence dependence involved in the best-estimate correlation employed for 15-15Ti claddings [38].
- The fission gas release increases rapidly after the high-power cycles at the beginning of irradiation and after approximately 330 days. A resulting increase in the pin pressure can be observed, although the post-INSPYRE TRANSURANUS version yields much lower values due to the coupling with SCIANTIX, as noticed and discussed for SUPERFACT-1 and RAPSODIE-I. The FGR and gap pressure predicted by the post-INSPYRE version of GERMINAL are highly influenced by the power variations, due to e.g., the effect of burst releases of fission gases.
- The evolution of the cladding outer radius deformation at the peak power node, reported in Figure 31, is similar in shape from the different codes, although TRANSURANUS predicts the strongest increase towards the end of life (coherent with the fuel-cladding gap evolution shown in Figure 30). The predicted behaviours in time do not seem very sensitive to the power variations. Irradiation-induced creep and irradiation-induced clad swelling dominate in the cladding profilometry evolution yielded by MACROS. Details about the modelling of these two phenomena in MACROS can be found in [39] and [40], respectively.

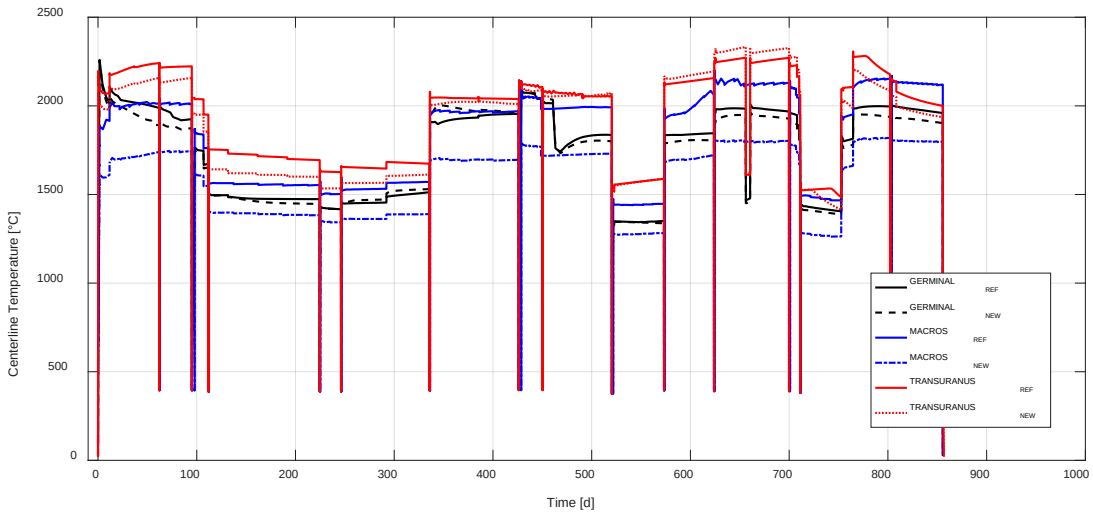

Figure 29: Fuel centreline temperature evolution of the NESTOR-3 110 pin at peak power node.

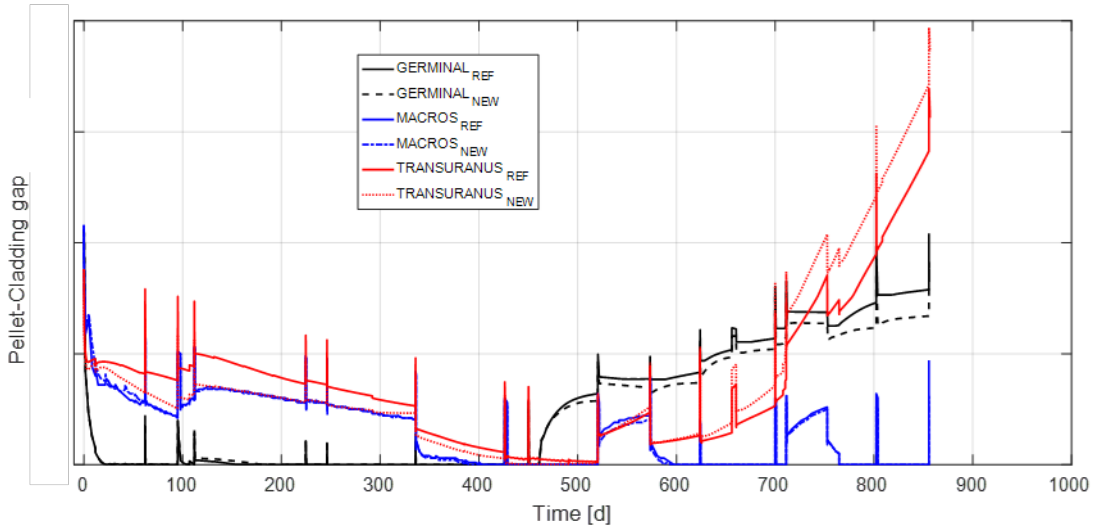

Figure 30: Pellet-cladding gap evolution of the NESTOR-3 110 pin at peak power node.

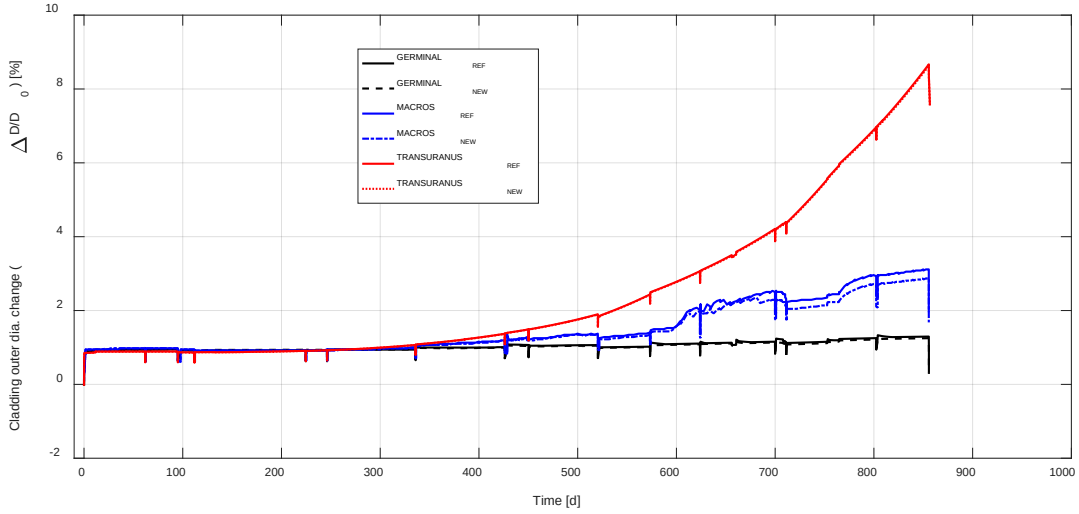

Figure 31: Cladding outer diameter variation for the NESTOR-3 110 pin at peak power node.

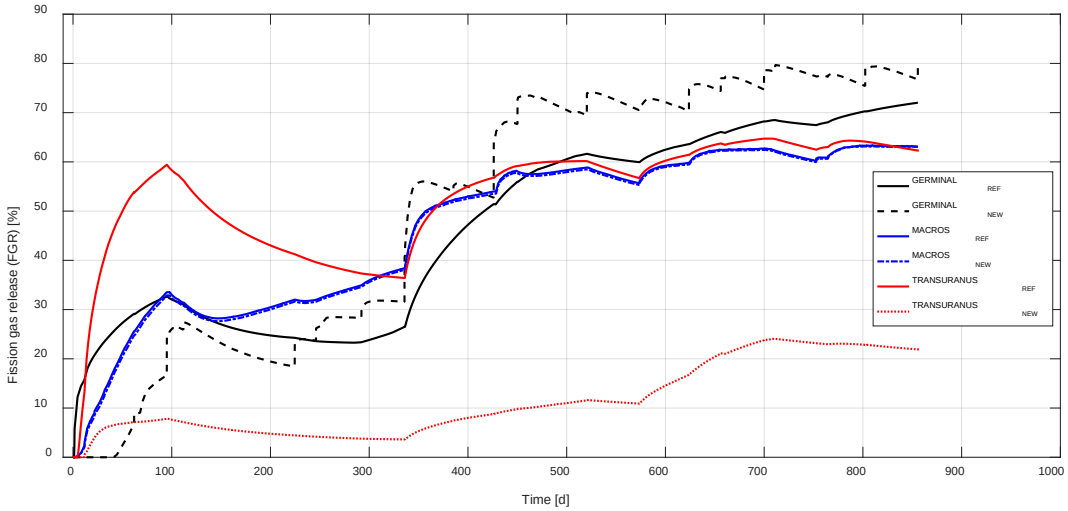

Figure 32: Fission gas release evolution of the NESTOR-3 110 pin at peak power node.

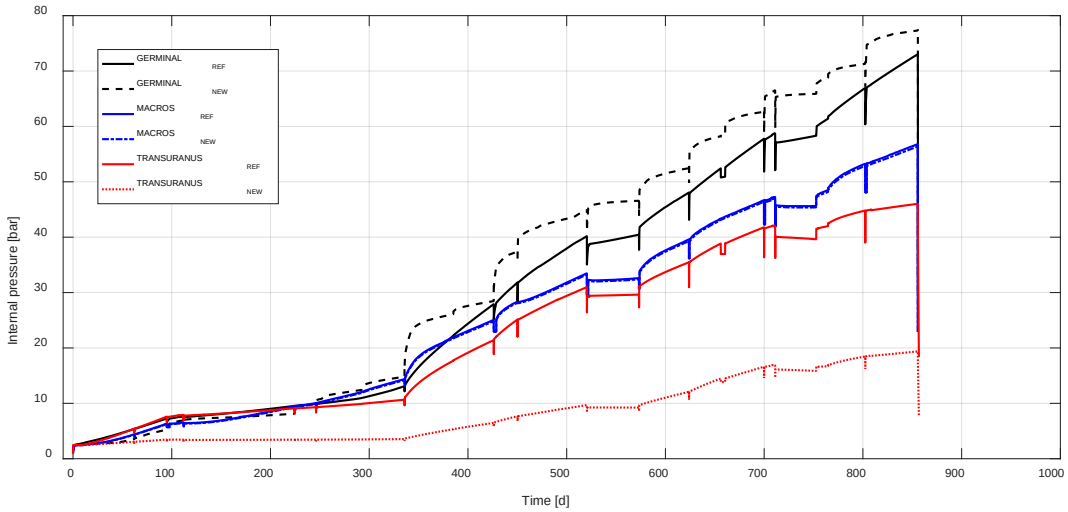

Figure 33. Pin pressure evolution of the NESTOR-3 110 pin at peak power node.

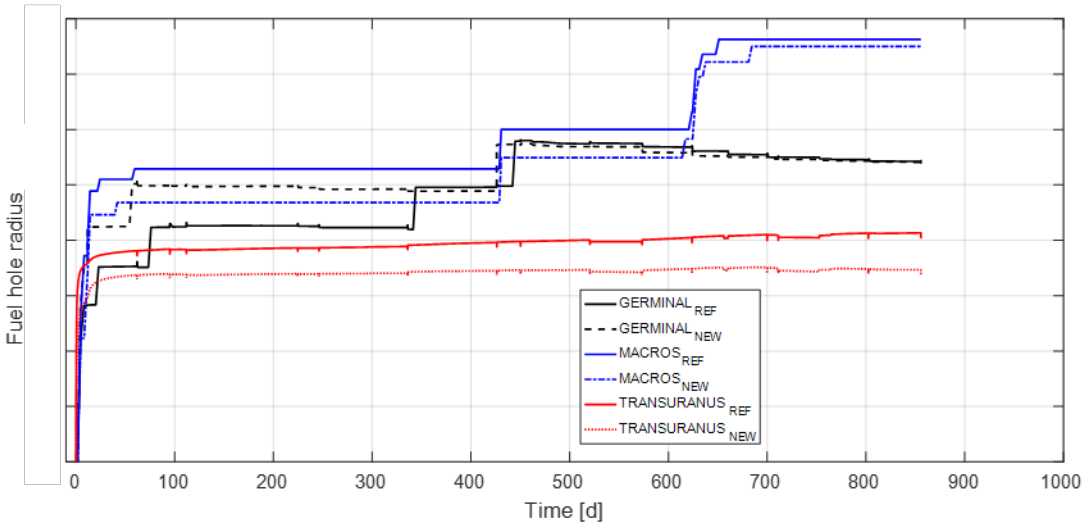

Figure 34: Fuel central hole radius evolution of the NESTOR-3 110 pin at peak power node.

4.2.2 Radial and axial profiles and comparison with experimental data

The axial profiles at the EOL yielded by the various code versions are compared with the experimental measurements in the figures below. The cladding diameter change is shown in Figure 35 and Figure 36, the central void radius in Figure 37, the columnar grain zone radius in Figure 38, the fuel outer radius in Figure 39 and the fuel-cladding gap size in Figure 40.

The cladding deformation magnitude measured and axial profile are relatively well estimated by MACROS and GERMINAL (Figure 35), while its magnitude is overestimated by TRANSURANUS, which seems to follow closely the shape of the axial flux profile. Given that the pellet-cladding gap remains open towards the end of irradiation, the contribution of radiation-induced creep to clad deformation should be limited and the differences should arise from the applied correlation for cladding swelling and from the JOG formation, as pointed out by the GERMINAL sensitivity study (Section 4.2.3). As swelling has a strong dependence on the fast neutron fluence, the impact of any uncertainty on the cladding damage dose (dpa) and on its conversion to fast neutron fluence is considerable, as already discussed in the analysis of the RAPSODIE-I irradiation experiment (Section 3.2).

A complementary test (Figure 36) reveals that an overall reduction of the fluence by 20-30%, which is compatible with the uncertainties on the measured power/neutron flux in fast reactor experiments [41], would lead to a satisfactory quantitative agreement of the TRANSURANUS predictions with the measured cladding deformation.

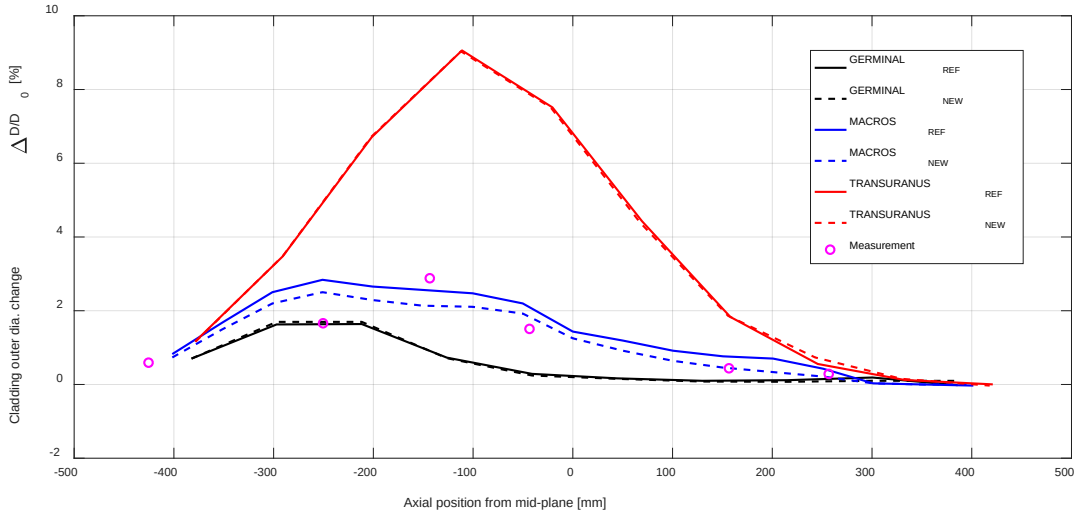

Figure 35: Axial profile of the cladding diameter change at the EOL of NESTOR-3 110 pin.

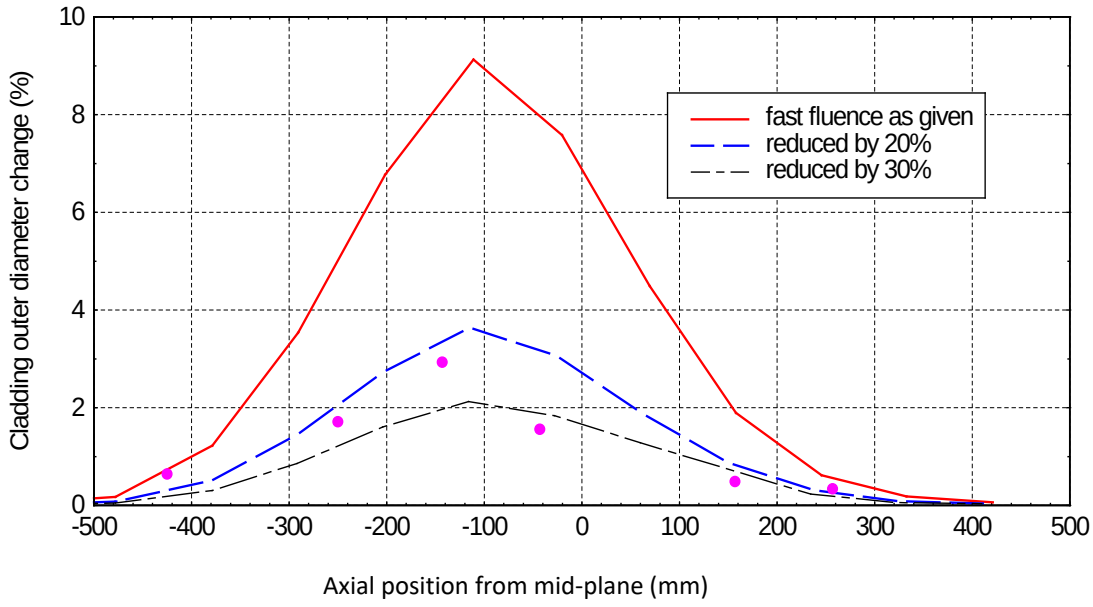

Figure 36: Axial profile of the cladding diameter change at the EOL of NESTOR-3 110 pin yielded by TRANSURANUS with various fast neutron fluences.

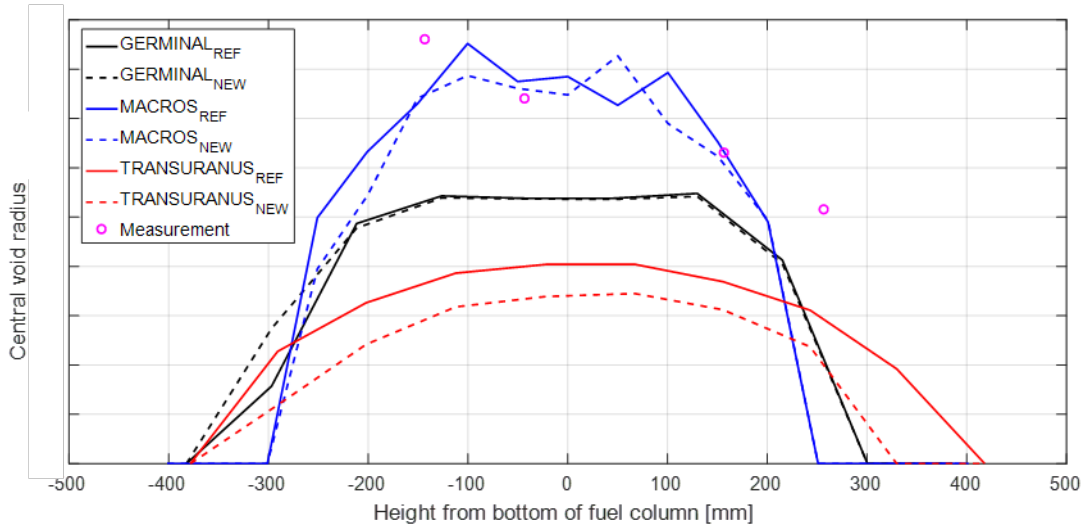

Figure 37: Axial profile of the fuel central void radius at the EOL of NESTOR-3 110 pin.

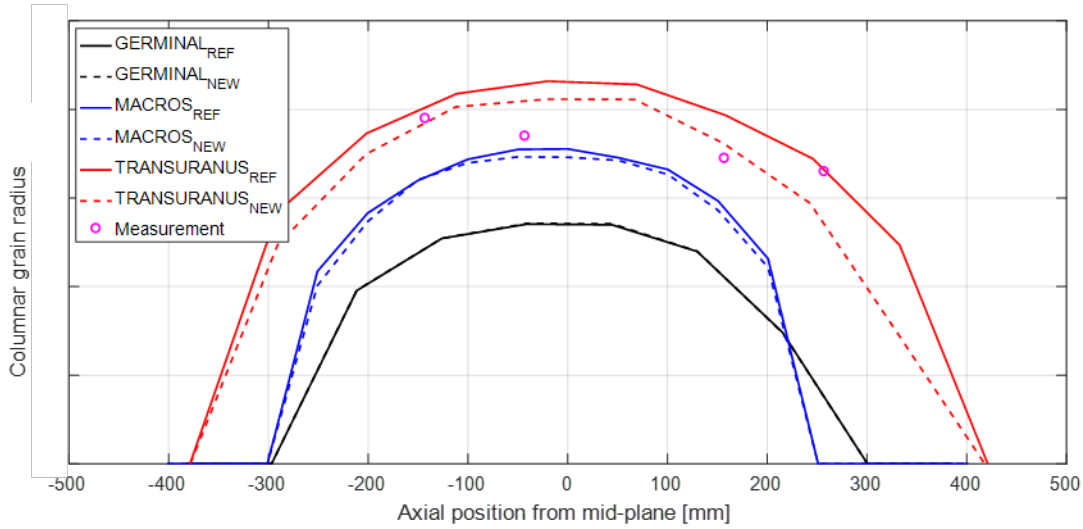

Figure 38: Axial profile of the columnar grain zone radius at the EOL of NESTOR-3 110 pin.

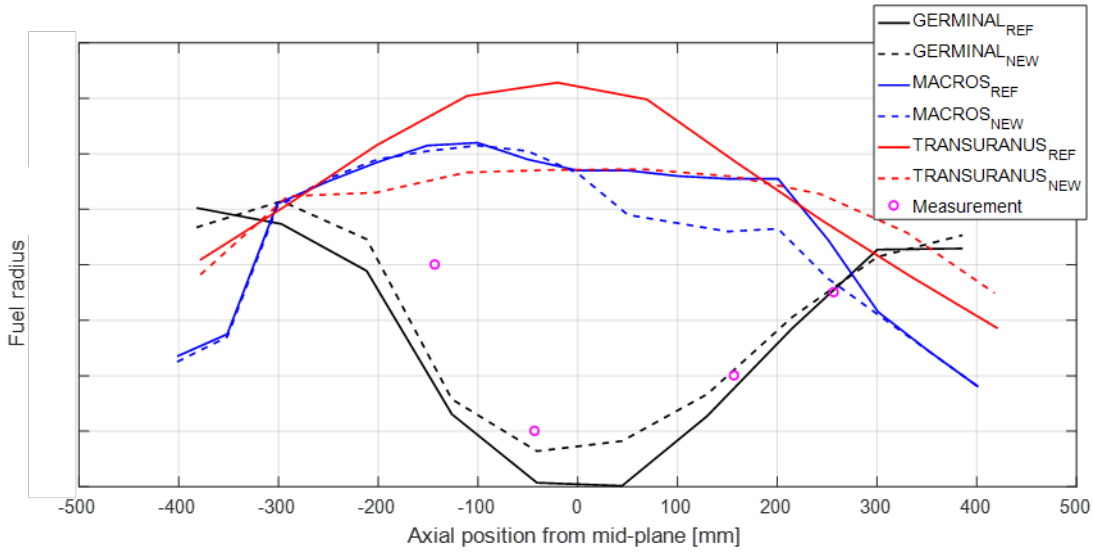

Figure 39: Axial profile of the fuel outer radius at the EOL of NESTOR-3 110 pin.

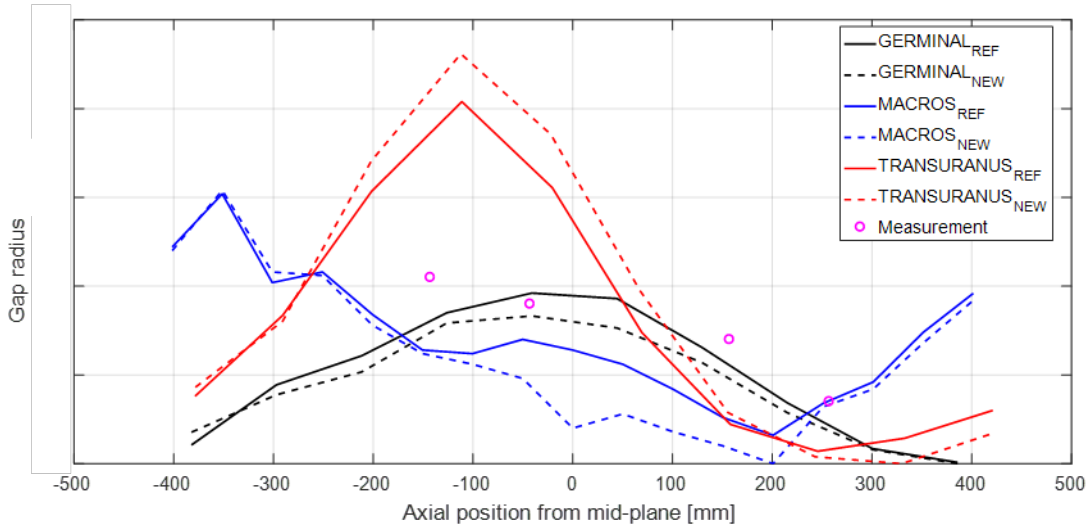

Figure 40: Axial profile of the fuel-cladding gap size at the EOL of NESTOR-3 110 pin.

The central void size is underestimated by GERMINAL and TRANSURANUS and well calculated by MACROS (Figure 37), although the MACROS code predicts no hole formation for the extreme regions of the fuel stack. The columnar grain zone size is captured best by the TRANSURANUS code.

The fuel outer radius (Figure 39) and pellet-cladding gap size (Figure 40) profiles yielded by GERMINAL are the only ones consistent with the experimental measurements. Combined with the peak in the radial caesium concentration, this would suggest the importance of taking into account the JOG for a correct modelling of fuel and cladding dimensional changes. As mentioned in Section 2.3, GERMINAL is the only code involved in INSPYRE that currently includes a model for the JOG formation and evolution in the fuel-cladding gap [9]. According to the experimental observations, the fuel-cladding gap at EOL is completely filled with JOG, determining the EOL gap size, which can explain the agreement of the GERMINAL results with the gap size measurements. Further details on the impact of the JOG model on the results is provided in Section 4.2.3 below.

The radial distribution of the Pu concentration at EOL is compared with measurements in Figure 41. It can be seen that no Pu redistribution model was used in the MACROS code (i.e., flat curve), while the two other code results are in satisfactory agreement with the measured profile.

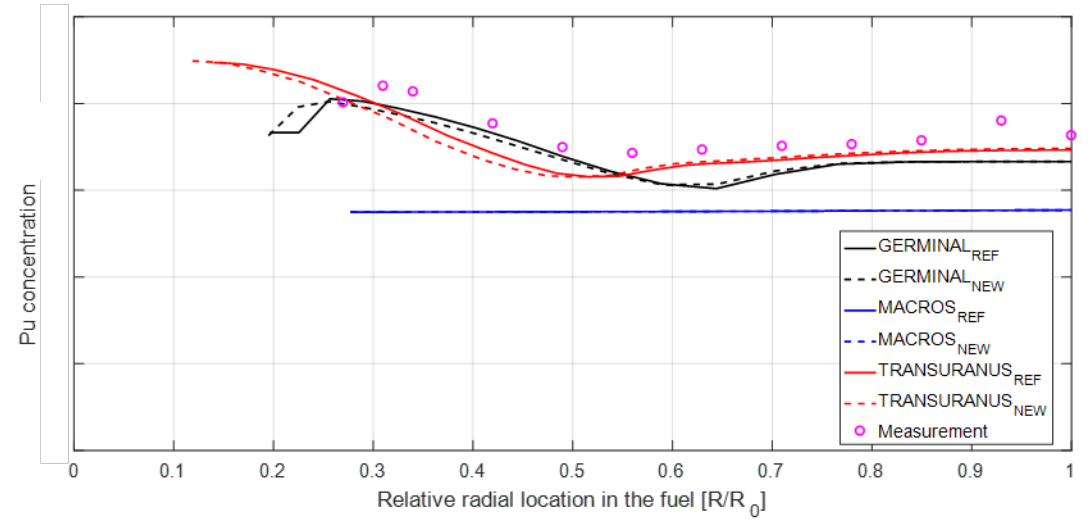

Figure 41: Radial profile of Pu concentration at the peak power node at the EOL of NESTOR-3 pin 110.

Table 7: Comparison of NESTOR-3 integral results with measurements (X: not calculated).
For the meaning of 'TU THERMAL', 'TU MECHANICAL' and 'TU SCIANTIX', see Section 2.3.

	Measured	TU REF	TU THERMAL	TU MECHANICAL	TU SCIANTIX	TU NEW	GERMINAL REF	GERMINAL NEW	MACROS REF	MACROS NEW
Fission gas (Xe+Kr) released @ STP (cm^3)	401	251.5	259.9	245.6	94.2	103.7	362.0	406.2	365.2	295.7
EOL He volume @ STP (cm^3)	38	22.6	14.3	14.3	X	X	40.2	42.4	42.4	30.3
Clad residual elongation (%)	0.3	2.3	2.0	2.0	2.0	2.0	0.2	0.0	0.00	0.4
Fuel residual elongation (%)	0.4	4.0	4.0	4.0	3.4	3.7	1.1	0.0	0.01	0.4

4.2.3 Integral code results and comparison with experimental data

The comparison between the integral values and measurements yielded by the codes is given in Table 7. TRANSURANUS code results are provided for various code settings, as described in Section 2.3.

Experimental data about the end-of-life fission gas release and helium content in the pin free volume were measured after 26 months of fuel storage after shutdown. Therefore, the reported value includes the initial filling, the release during irradiation and the decay during storage. The predictions by the involved codes generally under-estimate the experimental measurements, GERMINAL results being the closest to the experimental values.

As for the cladding and fuel residual elongations, experimental data are significantly overestimated by TRANSURANUS. The results of GERMINAL and MACROS are closer to the measurements. The MACROS code in its post-INSPYRE version proves to yield the best results, while the updated GERMINAL version predicts null EOL elongations.

4.3 Sensitivity studies

The objective of this sensitivity study is to analyse the sensitivity of integral quantities calculated to the JOG model implemented in GERMINAL, in order to get further insight into the differences between fuel performance codes identified in the benchmark study (see Section 4.2). To this aim, the results of calculations using the GERMINAL pre- and post-INSPYRE versions with or without the JOG model activated are compared with the fuel-cladding gap size data from the NESTOR-3 experiment.

The evolution under irradiation of the radial gap between fuel and cladding calculated with and without JOG model is shown in Figure 42. It can be observed that with the JOG model on, when the JOG formation occurs (at approximately 11000 h, i.e., 458 days), the fuel-cladding radial gap increases due to the formation of JOG in the gap. Then, after 11000 h, the gap evolution follows the increase of the JOG thickness. The impact of the JOG formation on the fuel central temperature is given in Figure 43. This shows that the fuel central temperature suddenly decreases at the beginning of the JOG formation compared to the behaviour obtained without the JOG model. The difference between the two temperatures calculated tends to decrease when the burnup increases (especially after 18000 h, i.e., 750 days). At the end of irradiation, the fuel central temperature with and without JOG model is almost the same. This can be explained if we consider the evolution of the pellet-to-cladding heat transfer coefficient. Before the JOG formation, the gap closes but the exchange coefficient is low due to the thermal resistance induced by the fission gases located in the free volume associated to the roughness of the pellet outer and cladding inner surfaces. Then, when the JOG layer starts to form, the JOG material, mostly caesium molybdate with a conductivity ten times greater, replaces fission gases. This explains the increase of the gap heat transfer coefficient and the decrease of the fuel central temperature. Then, the JOG layer thickness increases, reducing the thermal exchange coefficient between pellet and cladding. This leads to an increase in the fuel central temperature. At the end of irradiation, the heat transfer coefficient of the 80 microns thick JOG layer is comparable to that of a closed gap with fission gases, as can be concluded by the comparison with the results of GERMINAL without JOG model.

Figure 44 shows the axial profile of the radial gap size at the end of irradiation, corresponding to the JOG thickness profile. Without JOG model, a small, quasi-constant gap is predicted at the end of life because the pellet-cladding gap is closed before the final power shutdown. With the JOG model, the radial gap profile is given by the JOG thickness before the shutdown, in agreement with the evolution shown in Figure 42 for the peak power node.

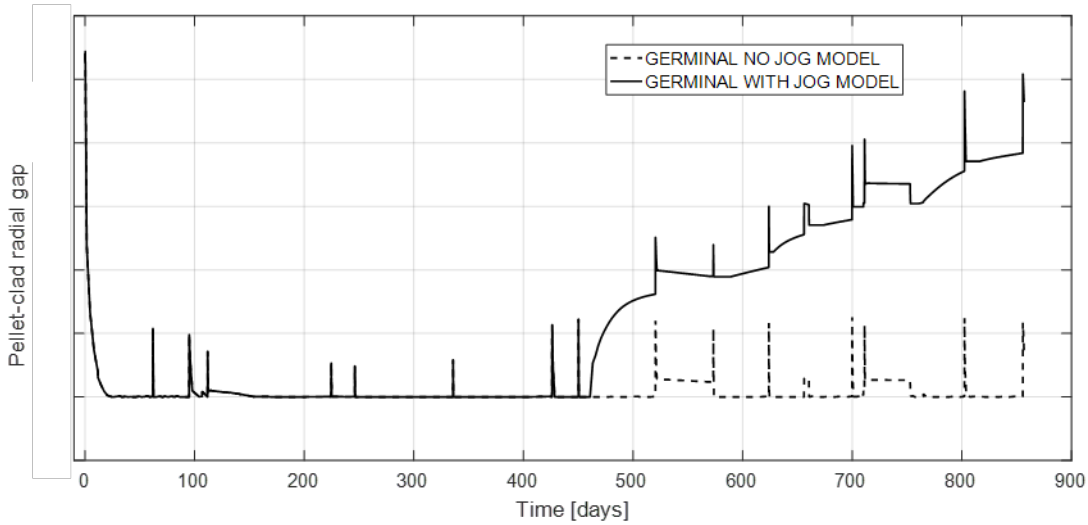

Figure 42: Evolution during irradiation of the radial fuel-cladding gap at the peak power node axial level yielded by GERMINAL with and without JOG modelling.

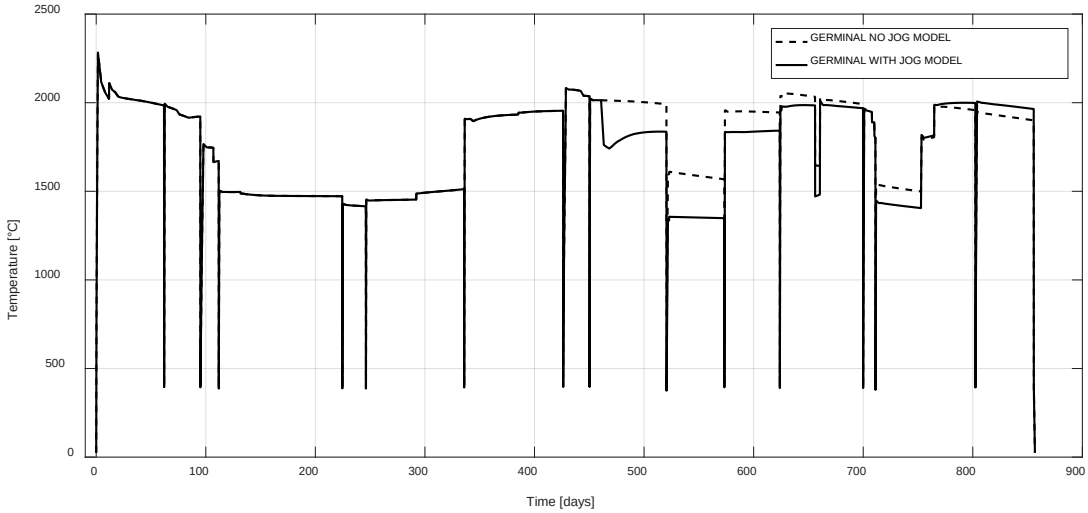

Figure 43: Evolution during irradiation of the fuel central temperature at the peak power node axial level yielded by GERMINAL with and without JOG modelling.

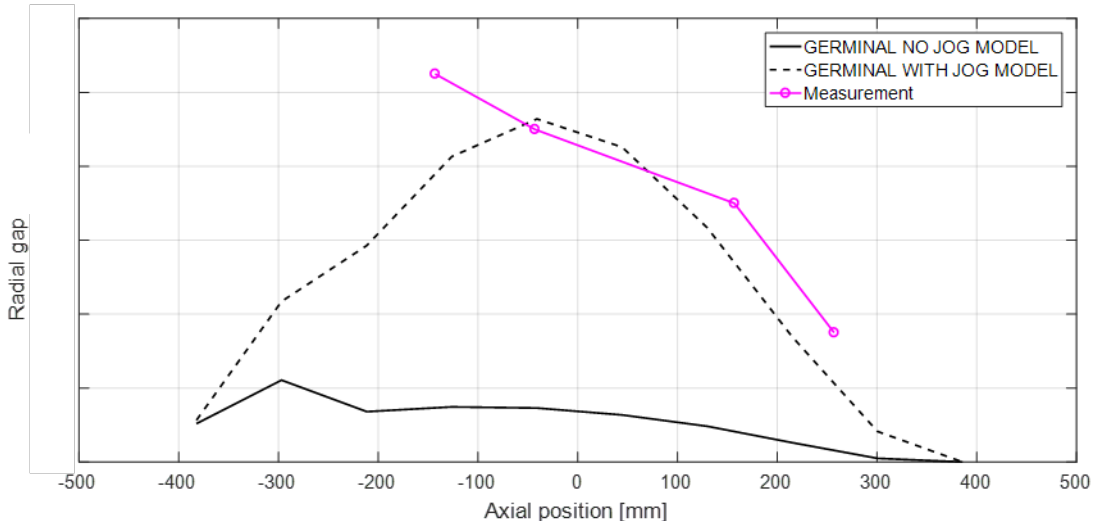

Figure 44: Axial profile of the fuel-cladding radial gap at the end of irradiation, predicted by GERMINAL with and without JOG modelling.

4.4 Conclusions on the NESTOR-3 simulation results

The assessment activity against the NESTOR-3 irradiation experiment points out an encouraging agreement between the predictions of the fuel performance codes involved and the available experimental data.

The differences in the results of the NESTOR-3 simulations between the pre- and post-INSPYRE versions of the TRANSURANUS, GERMINAL and MACROS codes are generally small. As already seen in the simulation of the two other irradiations, the current coupling of the SCIANTIX fission gas behaviour module with the TRANSURANUS code does not cover yet all the relevant fission products and release components and therefore the performed coupling of TRANSURANUS with SCIANTIX leads to an underestimation of the fission gas release and resulting inner pin pressure. Further developments are needed to combine the mechanisms for fission gas behaviour already implemented in TRANSURANUS with a subset of the SCIANTIX modelling appropriate for fast reactor conditions (e.g., limiting normal grain growth). In addition, SCIANTIX needs to be extended and assessed for FBR irradiation conditions.

Finally, the GERMINAL simulation results show that the JOG modelling affects positively the fuel and cladding end-of-life geometry and the gap width and conductance. This in turn influences the temperature inside the fuel and consequently the whole fuel pin thermal-mechanical performance. Therefore, based on this simulation case, further modelling advancements related to the JOG formation and evolution in MOX fuel under fast reactor irradiation conditions are of particular interest.

5 DISCUSSION ON THE IMPROVED CODE RESULTS

In this section, overall comparisons between reference and updated code results, together with the code assessment against the available experimental measurements, are discussed for the three irradiation experiments considered (SUPERFACT-1, RAPSODIE-1, NESTOR-3).
The items of particular interest for fast reactors conditions are the fuel restructuring, i.e., the columnar grains and central void formation, the fission gas release, the swelling-induced cladding deformations and the JOG formation and evolution in the fuel-cladding gap.

5.1 Fuel restructuring

The formation of columnar grains and of a central void region is a typical phenomenon observed experimentally observed in FBR MOX fuel at high temperature [42]. This restructuring of the fuel was found in all the three irradiation experiments simulated by the involved codes.

The SUPERFACT-1 fuel exhibited a central hole of about 0.7 mm in diameter while for the RAPSODIE-1 and NESTOR-3 experiments the central hole was significantly larger (~ 1.6 mm in diameter). The three codes (in both pre- and post-INSPYRE versions) are all capable of predicting the central hole formation with reasonable accuracy, MACROS predicting the largest hole size compared to the other two codes. The impact of the code improvements made in INSPYRE seems small on this parameter. The updated TRANSURANUS version predicts a smaller hole than the reference code version, typically leading to a further underestimation compared to the measured value.

5.2 Fission gas release

Fission gas release in fast reactor fuels can get close to 100% because of the high-power levels and the high fuel temperatures during operation. For the pins simulated, the FGR ranged from 70 to 80% at EOL.

The pre-INSPYRE codes seem already to predict this high level of FGR quite well (within +/- 10%). Some impact of the code modelling improvements performed in INSPYRE can be seen, although no clear trend of improvement can be identified.

The given implementation of SCIANTIX in TRANSURANUS leads to an unrealistic reduction of the fission gas release. Hence, the coupling scheme requires further changes to take into account fast reactor conditions (e.g. limiting normal grain growth), in line with what was done for the GERMINAL code in order to account for the fact that the SCIANTIX module was originally developed for LWR fuels.

Using GERMINAL post-INSPYRE version, the fission gas release is increased as well as the resulting internal pressure. This seems to be mainly due to the SCIANTIX inert gas model, which leads to a different gas release kinetics compared to the pre-INSPYRE version of GERMINAL. The post-INSPYRE version also yields a fission gas retention profile at EOL flatter than the experimental measurements. Too much gas release from the fuel periphery is observed and not enough release from the inner part of the pellet is obtained. The integration of SCIANTIX models in GERMINAL has a low impact on the final gas release amount, but yields a very different kinetic of gas release during irradiation and a spatial distribution of fission gas retention less consistent with experiment. This suggests that the description of the physical mechanisms in the high temperature regime needs to be improved.

5.3 Cladding deformation

The correct prediction of the clad deformation is challenging since it is the result of the interplay between pellet-cladding interaction, radiation-induced (and potentially thermal) creep and radiation-induced clad swelling.
The GERMINAL code yields good estimates of the magnitude and axial shape of the deformation for the SUPERFACT-1 and NESTOR-3 cases. The TRANSURANUS results are mostly driven by the axial shape of the neutron flux profile. The radiation-induced components dominate in the correlations applied and lead to an underestimation of the impact of the local temperature for the considered irradiation experiments. The MACROS results are in good agreement with the experimental data on NESTOR-3 and in reasonable agreement for the other two irradiation experiments.
The novel models of MOX fuel properties/phenomena developed in INSPYRE and implemented in the codes do not seem to make a big difference on the clad deformation and behaviour under irradiation. Further improvement of the predictions of this quantity should therefore be sought.

5.4 JOG formation

GERMINAL is the only of the three codes that already incorporates the modelling and impact of the JOG formation and evolution in the fuel-cladding gap of FBR pins. It was found in the simulation of the NESTOR-3 irradiation experiment that this could be key for a correct estimation of the pellet-cladding gap size evolution and the resulting impact on the fuel centreline temperature. There are also indications in the RAPSODIE-I experiment that the JOG may play role in the clad deformation and gap size since chemical compounds involving fission products were experimentally detected in the fuel-cladding gap. This effect, however, could not be verified using the two codes applied for the simulation of this irradiation (i.e., TRANSURANUS and MACROS) since they do not account for the JOG formation yet.

6 CONCLUSIONS

This report describes the assessment of the pre- and post-INSPYRE versions of the European fuel performance codes GERMINAL, MACROS and TRANSURANUS against local and integral experimental data from the three integral irradiation experiments SUPERFACT-1, RAPSODIE-1 and NESTOR-3.

The considered experimental pins (featuring U-Pu mixed oxide fuel, with small contents of the minor actinides Am and Np in the SUPERFACT-1 case) are representative for Generation IV fast reactors in terms of fuel composition, cladding material and irradiation conditions (i.e., temperature, linear power and neutron flux levels). The pre-INSPYRE versions of the involved codes were employed as well as the code versions improved during the INSPYRE Project (post-INSPYRE). The assessment of the simulation capabilities and validation of the codes is key for their future application in the design and safety assessment of fuel pins for Generation IV liquid metal-cooled reactor concepts.

6.1 Capabilities of pre-INSPYRE code versions

It was found that the three pre-INSPYRE code versions were capable of simulating the past experiments with a reasonable level of agreement between calculated and measured trends and values, regarding cladding deformation, fission gas release, fuel restructuring.
The predicted trends of key performance parameters, in particular temperature, FGR and clad deformation, are similar between the three codes. It is noted, however, that the magnitude of the differences between the values of some key safety parameters yielded by the various codes can be large. For example, the spread in the maximum fuel centreline temperature calculated reaches several hundreds of degrees Celsius.

6.2 Impact of the INSPYRE improvements on code results

The extensions of the GERMINAL, MACROS and TRANSURANUS codes are described in detail in the D.7.2 report [1]. In summary:

- The GERMINAL and TRANSURANUS codes were modified by integrating:
  - New correlations for MOX thermal conductivity, heat capacity (in GERMINAL) and melting temperature.
  - New correlations for MOX thermal expansion and Young's modulus.
  - The SCIANTIX inert gas behaviour module, coupled to the FPCs.
- MACROS changes concern the implementation of the new correlations for MOX thermal expansion and Young's modulus only.

Although the review and introduction of novel models and material properties for the MOX fuel properties in the codes is a step forward in the code extension, the resulting impact of the code modifications on the simulation of the three irradiation considered is limited. No clear improvement of the simulation results was identified. On the contrary, the coupling of the current version of the SCIANTIX code, initially developed for LWR conditions, with TRANSURANUS results in very low values for the fission gas release.

6.3 Recommendations and future work

Several code development paths and needed improvements related to the modelling of MOX fuels in fast reactor conditions are identified as a result of the code assessments presented in this report.

The results obtained suggest that, above all, modelling efforts are necessary to improve and harmonize the fuel temperature profile estimations yielded by the three codes. This would affect several temperature-driven phenomena, in particular the fuel thermal creep, which influences in turn the gap dynamics, the fission gas and helium behaviour and release, which would benefit from developments both on the modelling and on the experimental side. The results obtained with the TRANSURANUS code indicate the need to adapt further the mechanistic model for fission gas behaviour SCIANTIX to the operating conditions in Generation IV type of fuels. The integration of SCIANTIX models in the GERMINAL code paves the way, but the analysis of the radial profiles of fission products reveals room for improvement.

The radial profiles of various elements (Pu, Am, Np and O) also stressed the need to acquire better mobility data for the GERMINAL and TRANSURANUS codes. Concerning the MACROS code, the radial redistribution of some elements needs to be implemented. The recent results on plutonium diffusion presented in Deliverable D5.1 of the INSPYRE Project will be considered in future versions of the codes.

As pointed out by the different gap evolutions and related gap heat transfer calculated by the codes, additional accurate measurements concerning these parameters, especially for beginning-of-life conditions, would strongly support the modelling activity.

The need for consideration of the outer oxide layer between the fuel pellets and the cladding, generally referred to as the JOG, has also been pointed out at high burnup. GERMINAL is currently the only code modelling this phenomenon. A plan for the implementation of the additional JOG layer in the other codes (currently neglecting it) is proposed in Deliverable D6.5 of the INSPYRE Project.

The gap size is also affected by the irradiation behaviour of the stainless-steel cladding in liquid metal fast reactor conditions. Validation of radiation-induced clad swelling and creep can therefore also be identified as a topic to focus on, as suggested by the deviations among the code predictions of cladding profilometries and the corresponding sensitivity analysis.

Finally, the results of the code assessment presented in the present report reveal on the one hand the various developments needed by the current versions of fuel performance codes. On the other hand, they represent the basis for the evaluation of future improvements of the description of properties and phenomena specific to fast reactor fuel pins. This assessment is one the few examples currently available of joint application of fuel performance codes to the simulation of fast reactor irradiations. It calls for international collaborations devoted to the continuous improvement and integral validation of the codes for Generation IV fast reactors. A good example is the new coordinated research project of the IAEA on fuel materials for fast reactors [43], in which a code-to-code benchmark will also be performed.

REFERENCES

[1] P. Van Uffelen, A. Schubert, L. Luzzi, T. Barani, A. Magni, D. Pizzocri, M. Lainet, V. Marelle, B. Michel, B. Boer, S. Lemehov, and A. Del Nevo, "Incorporation and verification of models and properties in fuel performance codes", INSPYRE Deliverable D7.2, 2020.

[2] L. Luzzi, T. Barani, A. Magni, D. Pizzocri, A. Schubert, P. Van Uffelen, M. Bertolus, V. Marelle, B. Michel, B. Boer, S. Lemehov, and A. Del Nevo, "Report describing the Irradiation Experiments selected for the Assessment of Fuel Performance Codes", INSPYRE Deliverable D7.1, 2019.

[3] J.-F. Babelot and N. Chauvin, "Joint CEA/JRC Synthesis Report of the Experiment SUPERFACT 1", Report JRC-ITU-TN-99/03, 1999.

[4] C. Prunier, F. Boussard, L. Koch, and M. Coquerelle, "Some specific aspects of homogeneous Am and Np based fuels transmutation through the outcomes of the SUPERFACT experiment in Phenix fast reactor", in: *Global '93: international conference and technology exhibition*, 12-17 September 1993, Seattle, WA, USA, 1993.

[5] C. T. Walker and G. Nicolaou, "Transmutation of neptunium and americium in a fast neutron flux: EPMA results and KORIGEN predictions for the SUPERFACT fuels", *J. Nucl. Mater.*, vol. 218, no. 2, pp. 129–138, 1995.

[6] T. Preusser and K. Lassmann, "Current Status of the Transient Integral Fuel Element Performance Code URANUS", in: *SMiRT 7*, 22-26 August 1983, Chicago, USA 1983.

[7] K. Lassmann and F. Hohlefeld, "The revised URGAP model to describe the gap conductance between fuel and cladding", *Nucl. Eng. Des.*, vol. 103, no. 2, pp. 215–221, 1987.

[8] European Commission, *TRANSURANUS Handbook*, Joint Research Centre, Karlsruhe, Germany, 2020.

[9] M. Lainet, B. Michel, J. C. Dumas, M. Pelletier, and I. Ramière, "GERMINAL, a fuel performance code of the PLEIADES platform to simulate the in-pile behaviour of mixed oxide fuel pins for sodium-cooled fast reactors", *J. Nucl. Mater.*, vol. 516, pp. 30–53, 2019.

[10] C. F. Clement, "The movement of lenticular pores in UO_2 nuclear fuel elements", *J. Nucl. Mater.*, vol. 68, no. 1, pp. 63–68, 1977.

[11] C. Ronchi and C. Sari, "Properties of lenticular pores in UO_2, $(U,Pu)O_2$ and PuO_2", *J. Nucl. Mater.*, vol. 50, no. 1, pp. 91–97, 1974.

[12] W. Dienst, I. Muelle-Lyda, and H. Zimmermann, "Swelling, densification and creep of oxide and carbide fuels under irradiation", in: *International conference on fast breeder reactor performance*, 5-8 March 1979, Monterey, CA, USA, 1979.

[13] S. E. Lemehov, F. Jutier, Y. Parthoens, B. Vos, S. Van Den Berghe, M. Verwerft, and N. Nakae, "MACROS benchmark calculations and analysis of fission gas release in MOX with high content of plutonium," *Prog. Nucl. Energy*, vol. 57, pp. 117–124, 2012.

[14] T. C. Chawla, D. L. Graff, R. C. Borg, G. L. Bordner, D. P. Weber, and D. Miller, "Thermophysical properties of mixed oxide fuel and stainless steel type 316 for use in transition phase analysis", *Nucl. Eng. Des.*, vol. 67, no. 1, pp. 57–74, 1981.

[15] G. Pastore, L. Luzzi, V. Di Marcello, and P. Van Uffelen, "Physics-based modelling of fission gas swelling and release in UO_2 applied to integral fuel rod analysis", *Nucl. Eng. Des.*, vol. 256, pp. 75–86, 2013.

[16] H. Többe, "Das Brennstabrechenprogramm IAMBUS zur Auslegung von Schellbrüter Brennstäben", Interatom - Technischer Bericht 75.65, 1975.

[17] A. Gallais-During, F. Delage, S. Béjaoui, S. Lemehov, J. Somers, D. Freis, W. Maschek, S. Van Til, E. D'Agata, and C. Sabathier, "Outcomes of the PELGRIMM project on Am-bearing fuel in pelletized and spherepac forms", *J. Nucl. Mater.*, vol. 512, pp. 214–226, 2018.

[18] M. Temmar, B. Michel, I. Ramiere, and N. Favrie, "Multi-physics modelling of the pellet-to-cladding gap closure phenomenon for SFR fuel performance codes", *J. Nucl. Mater.*, vol. 529, 151909, 2020.

[19] V. Di Marcello, A. Schubert, J. Van De Laar, and P. Van Uffelen, "Extension of the TRANSURANUS plutonium redistribution model for fast reactor performance analysis", *Nucl. Eng. Des.*, vol. 248, pp. 149–155, 2012.

[20] M. Bober, C. Sari, and G. Schumacher, "Redistribution of plutonium and uranium in mixed (U, Pu) oxide fuel materials in a thermal gradient", *J. Nucl. Mater.*, vol. 39, no. 3, pp. 265–284, 1971.

[21] C. F. Clement and M. W. Finnis, "Plutonium redistribution in mixed oxide (U, Pu)O_2 nuclear fuel elements", *J. Nucl. Mater.*, vol. 75, no. 1, pp. 193–200, 1978.

[22] D. Olander, *Fundamental aspects of nuclear reactor fuel elements*, Dept. of Nuclear Engineering, California University, Berkeley, USA, 1976.

[23] P. Konarski, J. Sercombe, C. Riglet-Martial, L. Noirot, I. Zacharie-Aubrun, K. Hanifi, M. Frégonèse, and P. Chantrenne, "3D simulation of a power ramp including fuel thermochemistry and oxygen thermodiffusion," *J. Nucl. Mater.*, vol. 519, pp. 104–120, 2019.

[24] P. Chakraborty, C. Guéneau, and A. Chartier, "Development of a complete thermo-kinetic description of cations in the mixed oxide of uranium and plutonium", in: *NuFuel 2019 Workshop*, 4-7 November 2019, PSI Villigen, Switzerland, 2019.

[25] M. Kato, K. Maeda, T. Ozawa, M. Kashimura, and Y. Kihara, "Physical properties and irradiation behavior analysis of Np- and Am-Bearing MOX Fuels", *J. Nucl. Sci. Technol.*, vol. 48, no. 4, pp. 646–653, 2011.

[26] V. Di Marcello, V. Rondinella, A. Schubert, J. van de Laar, and P. Van Uffelen, "Modelling actinide redistribution in mixed oxide fuel for sodium fast reactors", *Prog. Nucl. Eng.*, vol. 72, pp. 83–90, 2014.

[27] R. Parrish and A. Aitkaliyeva, "A review of microstructural features in fast reactor mixed oxide fuels", *J. Nucl. Mater.*, vol. 510, pp. 644–660, 2018.

[28] T. Barani, D. Pizzocri, F. Cappia, L. Luzzi, G. Pastore, and P. Van Uffelen, "Modeling high burnup structure in oxide fuels for application to fuel performance codes. Part I: High burnup structure formation", *J. Nucl. Mater.*, vol. 539, 152296, 2020.

[29] D. Pizzocri, F. Cappia, L. Luzzi, G. Pastore, V. V. Rondinella, and P. Van Uffelen, "A semi-empirical model for the formation and depletion of the high burnup structure in UO_2", *J. Nucl. Mater.*, vol. 487, pp. 23-29, 2017.

[30] F. Cappia, D. Pizzocri, A. Schubert, P. Van Uffelen, G. Paperini, D. Pellottiero, R. Macián-Juan, and V. V. Rondinella, "Critical assessment of the pore size distribution in the rim region of high burnup UO_2 fuels", *J. Nucl. Mater.*, vol. 480, pp. 138–149, 2016.

[31] J. Noirot, L. Desgranges, and J. Lamontagne, "Detailed characterization of high burn-up structures in oxide fuels," *J. Nucl. Mater.*, vol. 372, no. 2–3, pp. 318–339, 2008.

[32] V. V. Rondinella and T. Wiss, "The high burn-up structure in nuclear fuel", *Mater. Today*, vol. 13, no. 12, pp. 24–32, 2010.

[33] A. Magni, T. Barani, A. Del Nevo, D. Pizzocri, D. Staicu, P. Van Uffelen, and L. Luzzi, "Modelling and assessment of thermal conductivity and melting behaviour of MOX fuel for fast reactor applications", *J. Nucl. Mater.*, vol. 541, 152410, 2020.

[34] J. B. Ainscough, B. W. Oldfield, and J. O. Ware, "Isothermal grain growth kinetics in sintered UO2 pellets", *J. Nucl. Mater.*, vol. 49, no. 2, pp. 117–128, 1973.

[35] D. Haas, J. Van Velde, M. Gaube, J. Ketels, and C. Van Loon, "Results of the Postirradiation Examinations of the RAPSODIE-I Experiment Fuel Pins", *Nucl. Technol.*, vol. 34, pp. 75–88, 1977.

[36] P. Verbeek, H. Tobbe, N. Hoppe, and B. Steinmetz, "Liquid-Metal Fast Breeder reactor fuel rod performance and modeling at high burnup", *Nucl. Technol.*, vol. 39, pp. 167–185, 1978.

[37] D. Haas, J. Van de Velde, C. Van Loon, and J. Ketels, "RAPSODIE experiment post irradiation report, part 3 : Destructive examinations of the fuel pins", SCK CEN Report, 1977.

[38] L. Luzzi, A. Cammi, V. Di Marcello, S. Lorenzi, D. Pizzocri, and P. Van Uffelen, "Application of the TRANSURANUS code for the fuel pin design process of the ALFRED reactor", *Nucl. Eng. Des.*, vol. 173, no. 277, 2014.

[39] H.-J. Bergmann, "Projekt-Materialdatenhandbuch KNK II/3, Revisionsstand 04/88", INTERATOM GmbH, Bergisch-Gladbach, Germany, 1988.

[40] S. E. Lemehov, V. P. Sobolev, and M. Verwerft, "Predicting thermo-mechanical behaviour of high minor actinide content composite oxide fuel in a dedicated transmutation facility", *J. Nucl. Mater.*, vol. 416, no. 1–2, pp. 179–191, Sep. 2011.

[41] B. Boer, "Simulation of the RAPSODIE fuel pin irradiations with the TRANSURANUS code", SCK CEN, no. R-6273, 2017.

[42] F. Cappia, K. Tanaka, M. Kato, K. McClellan, and J. Harp, "Post-irradiation examinations of annular mixed oxide fuels with average burnup 4 and 5% FIMA", *J. Nucl. Mater.*, vol. 533, 152076, 2020.

[43] IAEA, "Coordinated Research Project - Fuel Materials for Fast Reactors", 2019. [Online]. Available: *https://www.iaea.org/projects/crp/t12031*.

[44] OECD/NEA, "Primary Radiation Damage in Materials", Report NEA/NSC/DOC(2015)9, 2015.

APPENDIX A RESULTS ON SUPERFACT-1 SF16 PIN

The figures below present the code results from the simulation of the SUPERFACT-1 SF16 pin (Am-bearing MOX). The correlations employed by the codes are the same as for the simulation of the Np-bearing pin SF13, whose results are shown in Section 2.3.

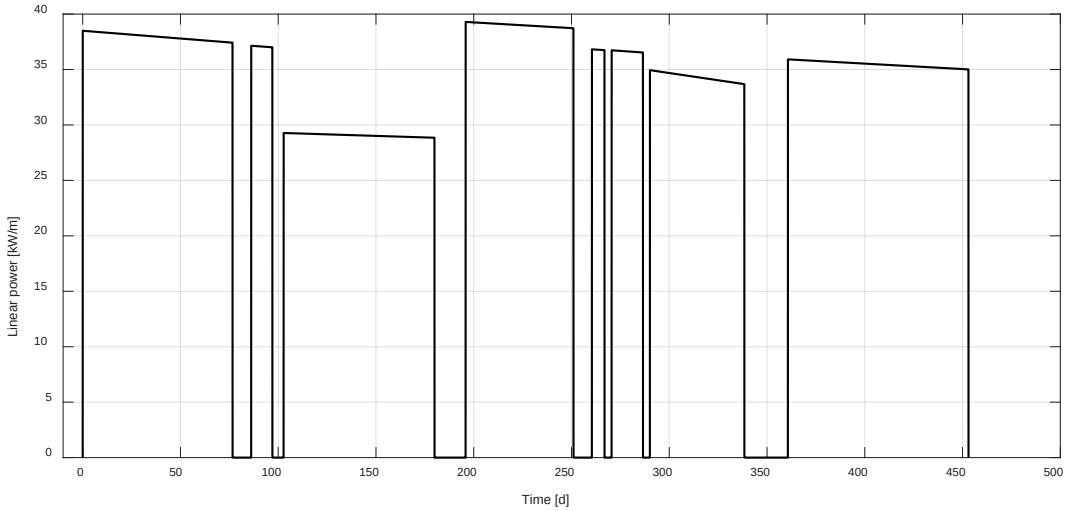

Figure 45. Power history of the SUPERFACT-1 experiment for fuel pin SF16 at the peak power node.

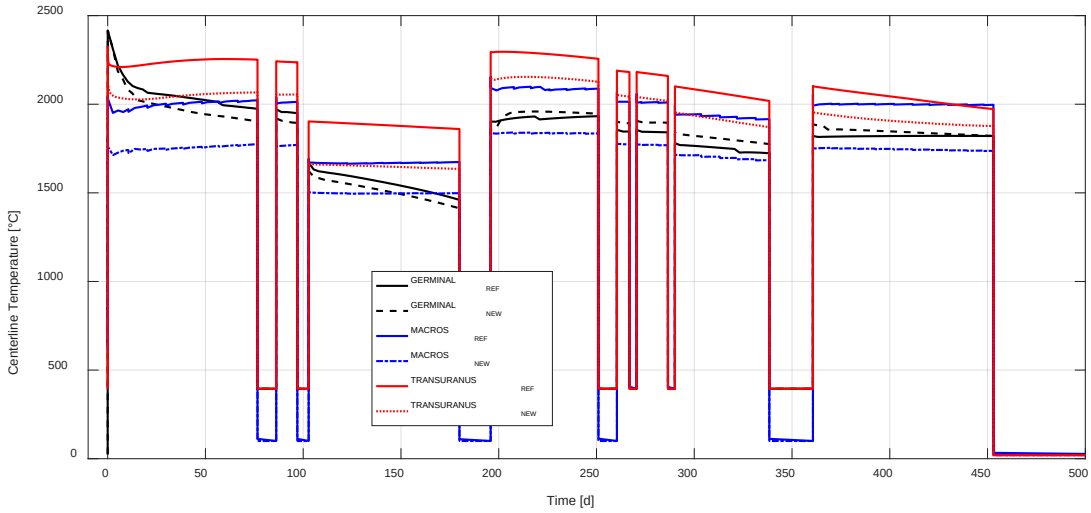

Figure 46. Fuel centreline temperature evolution of the SUPERFACT-1 SF16 pin at peak power node.

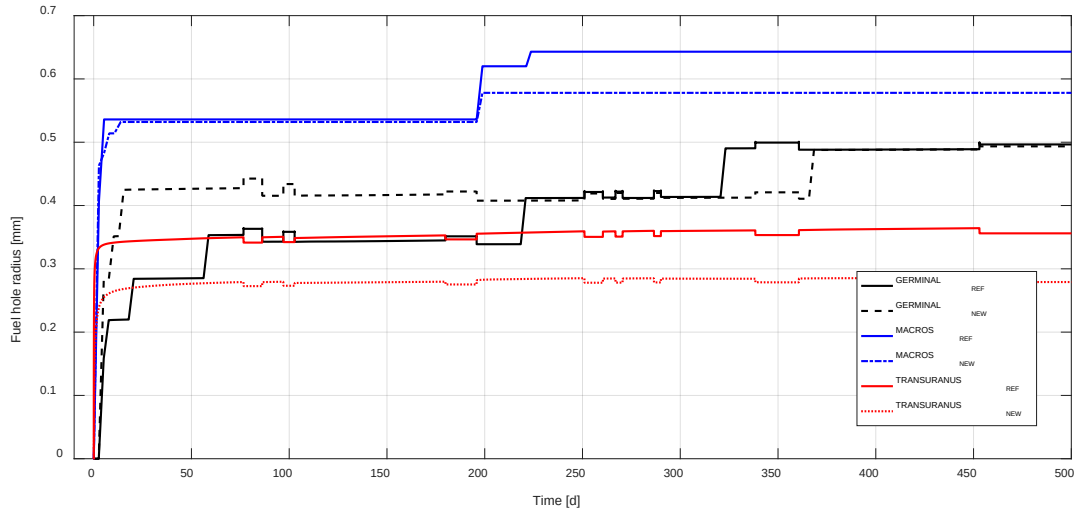

Figure 47. Fuel inner radius (hole) evolution during the SUPERFACT-1 experiment for SF16 fuel pin at peak power node.

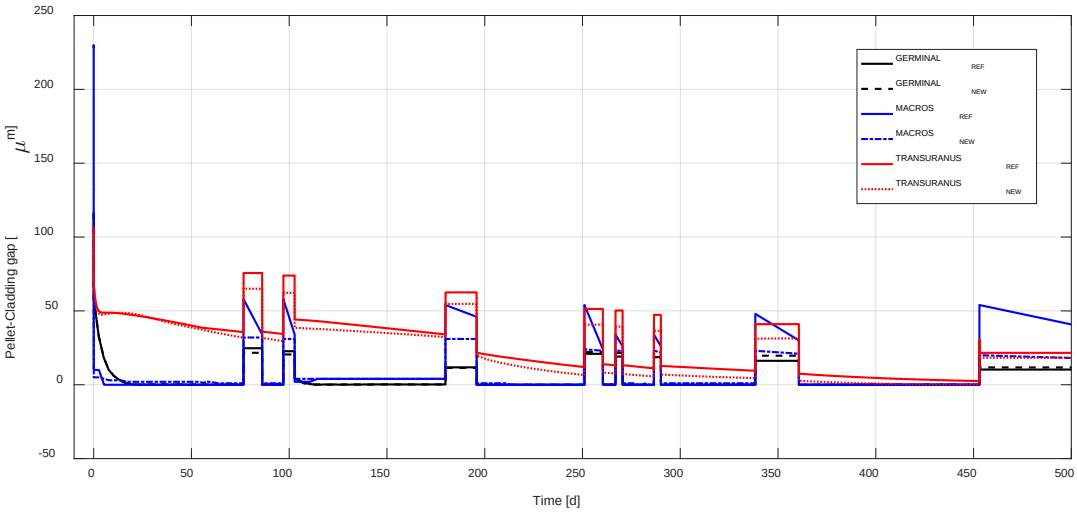

Figure 48. Fuel-cladding gap size evolution of the SUPERFACT-1 SF16 pin at peak power node.

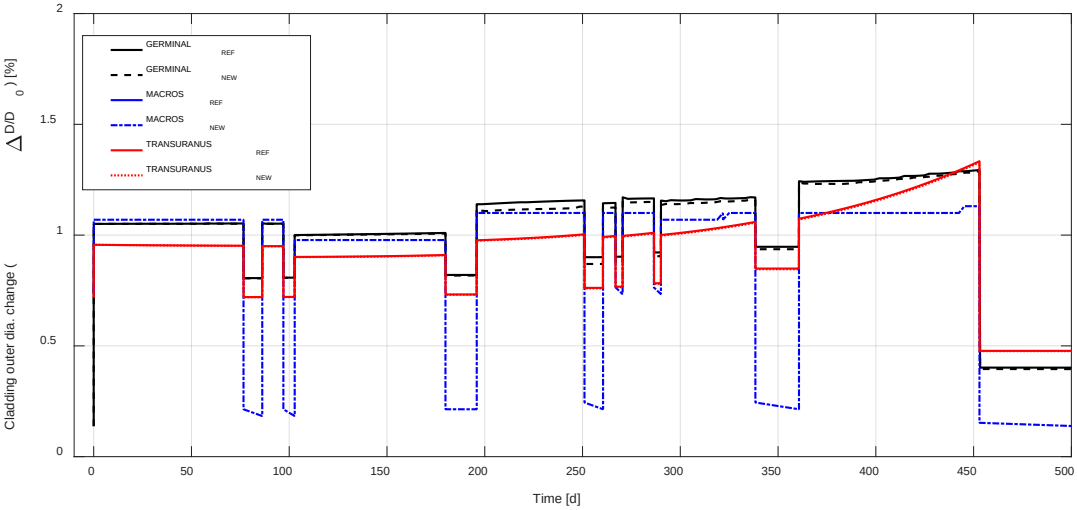

Figure 49. Cladding diameter change evolution of the SUPERFACT-1 SF16 pin at peak power node.

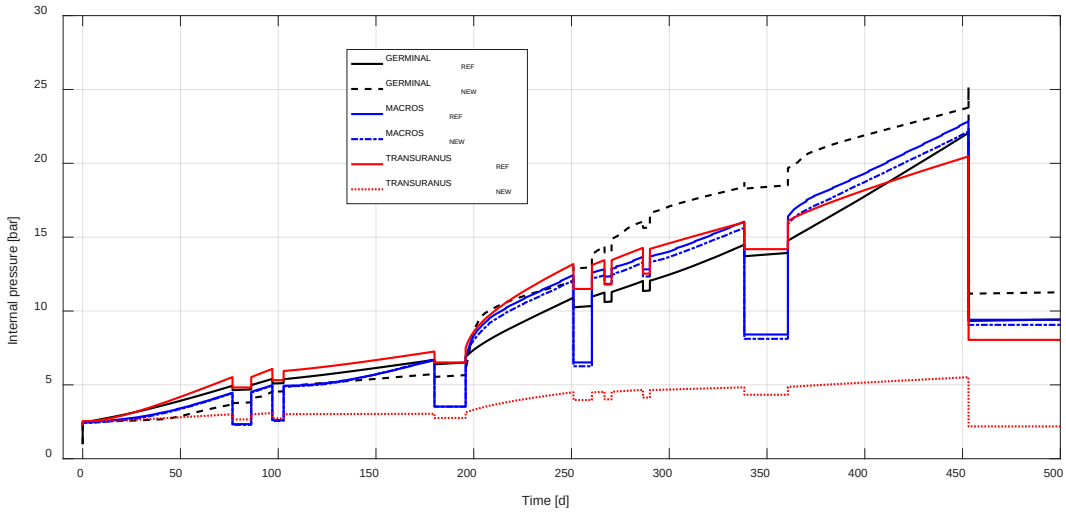

Figure 50. Inner pin pressure evolution of the SUPERFACT-1 SF16 pin at the peak power node.

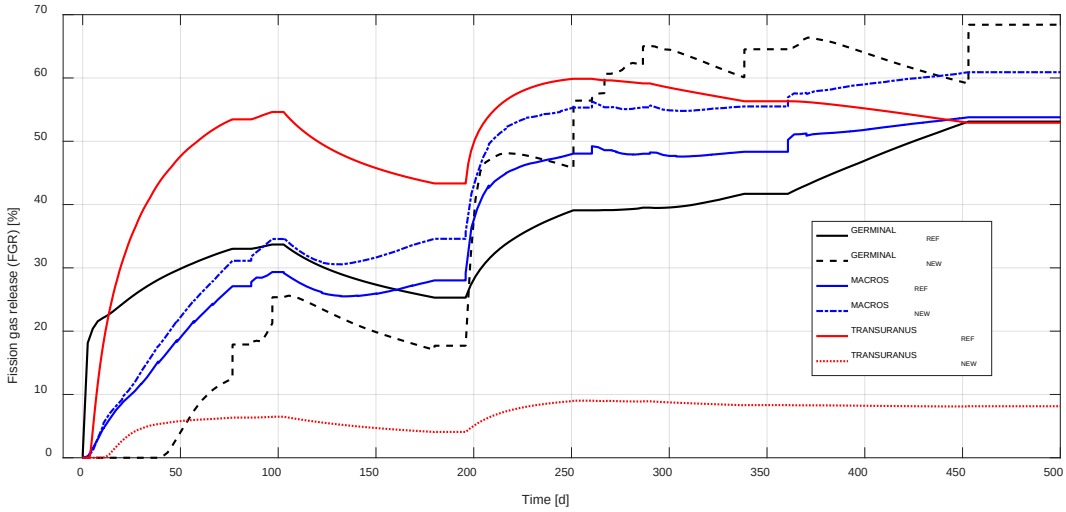

Figure 51. Fission gas release for SUPERFACT-1 SF16 fuel pin at peak power node.

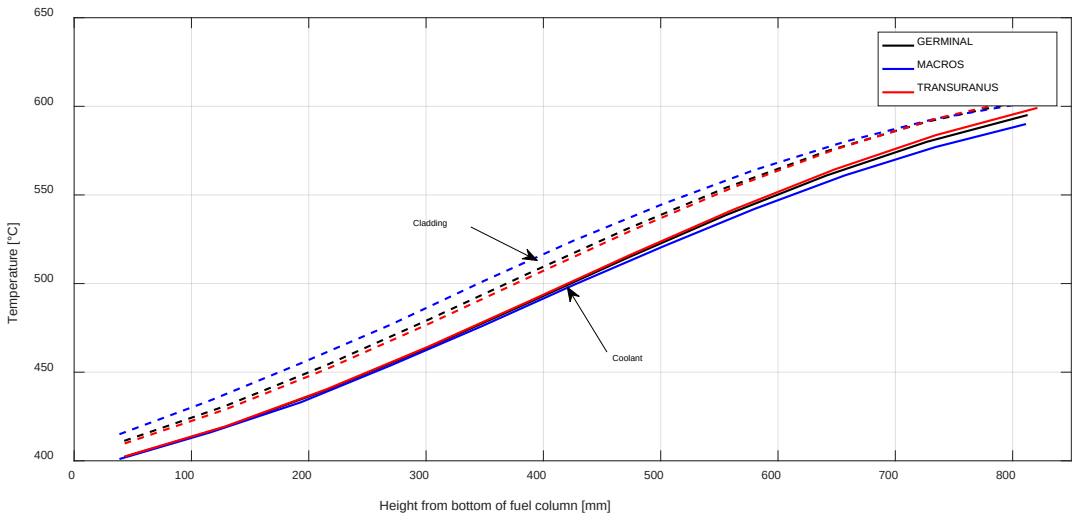

Figure 52. Axial profiles of the cladding and coolant temperature for SF16 fuel pin after 1 hour of operation during the SUPERFACT-1 experiment.

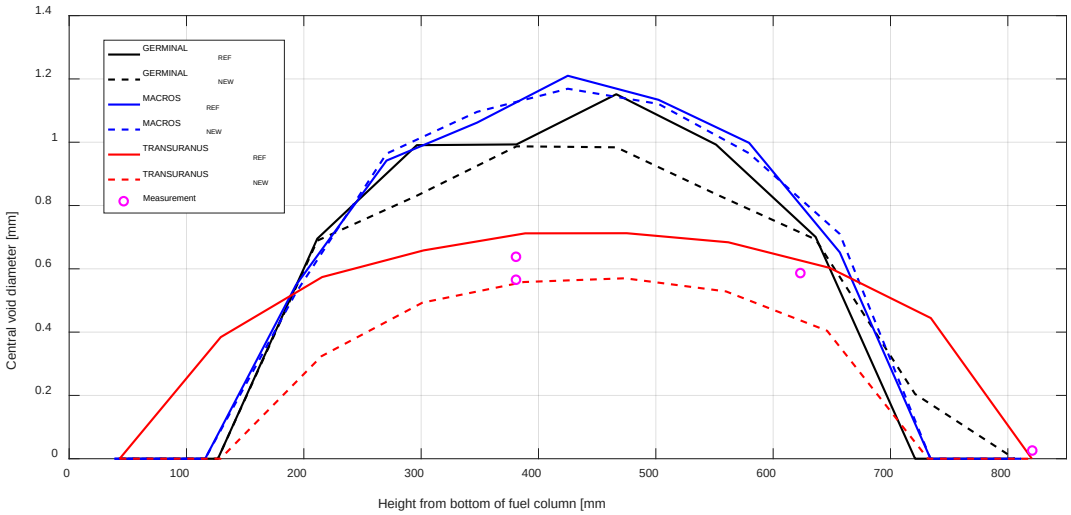

Figure 53. Axial profiles of the fuel central void diameter of the SUPERFACT-1 SF16 pin at end of life.

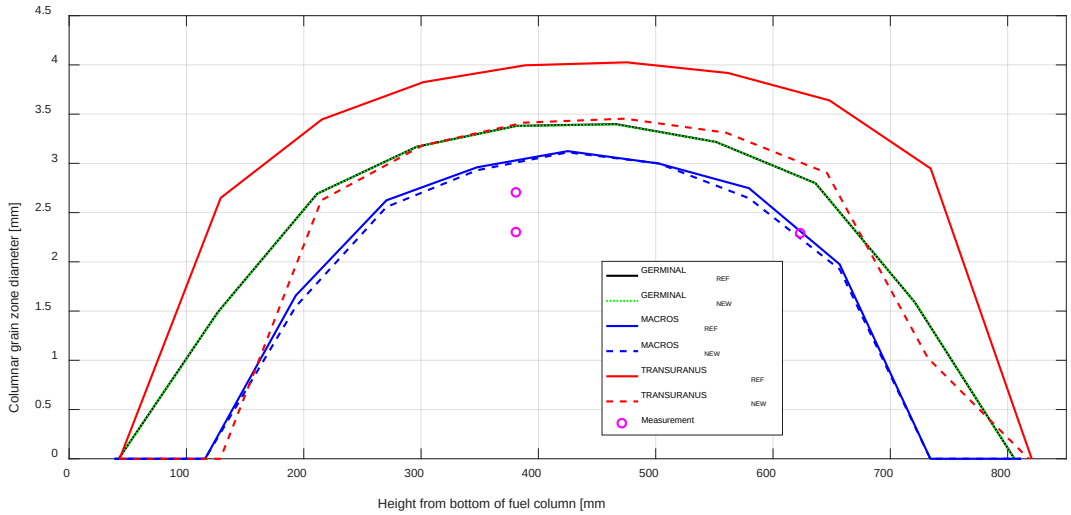

Figure 54. Axial profiles of the diameter of the columnar grain zone of the SUPERFACT-1 SF16 pin at end of life.

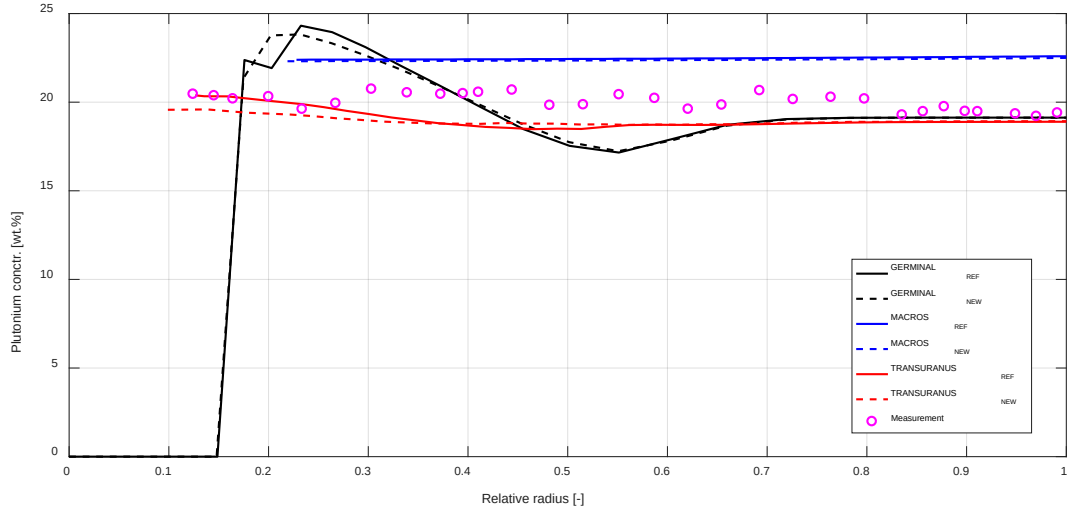

Figure 55. Radial profiles of the plutonium concentration of the SUPERFACT-1 pin SF16 at end of life.

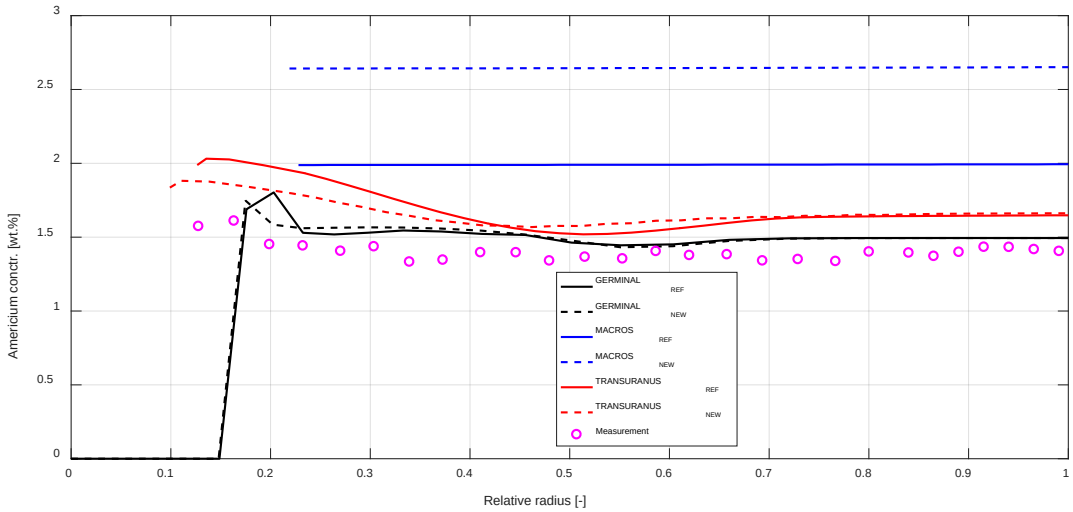

Figure 56. Radial profiles of the neptunium concentration of the SUPERFACT-1 pin SF16 at end of life.

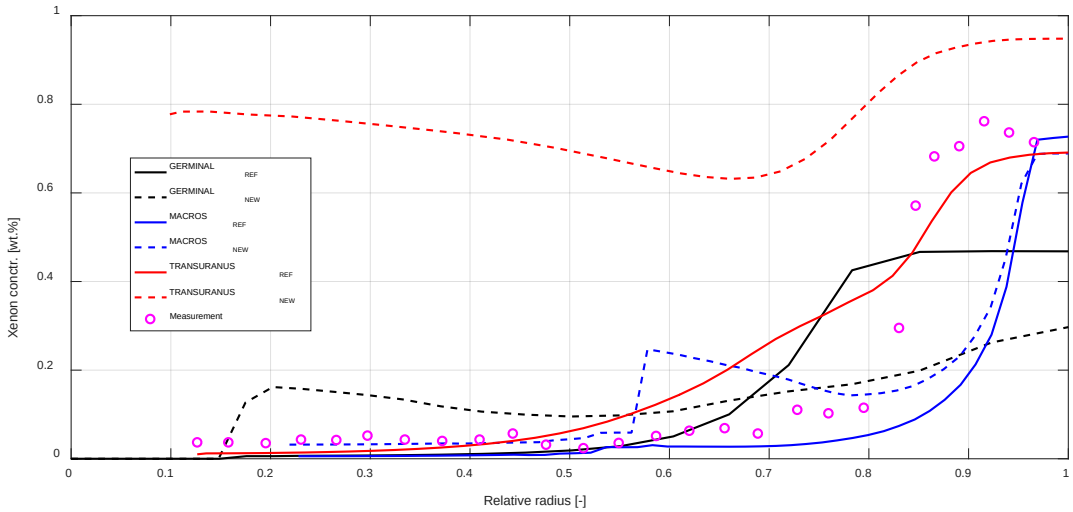

Figure 57. Radial profiles of the xenon concentration of the SUPERFACT-1 pin SF16 at end of life.

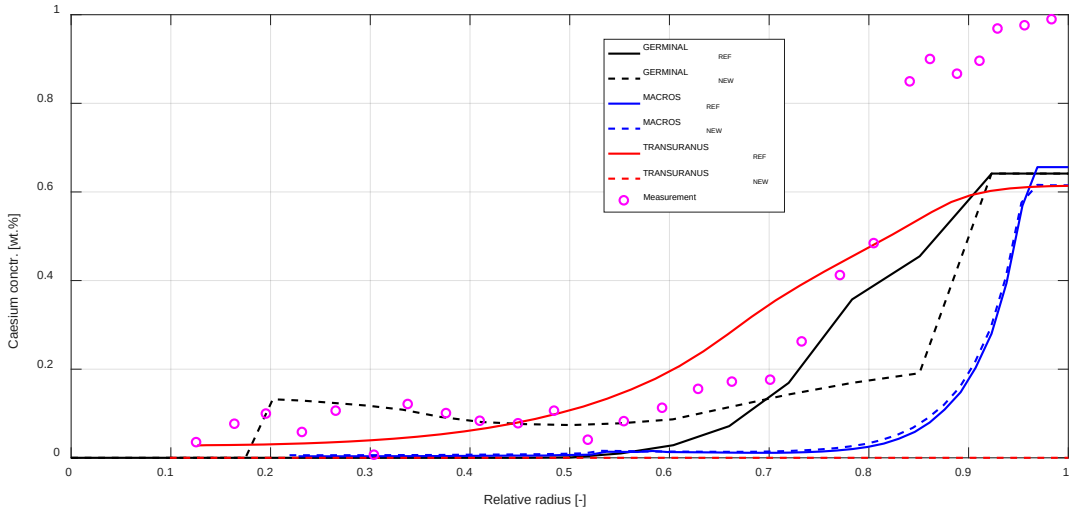

Figure 58. Radial profiles of the caesium concentration of the SUPERFACT-1 pin SF16 at end of life.

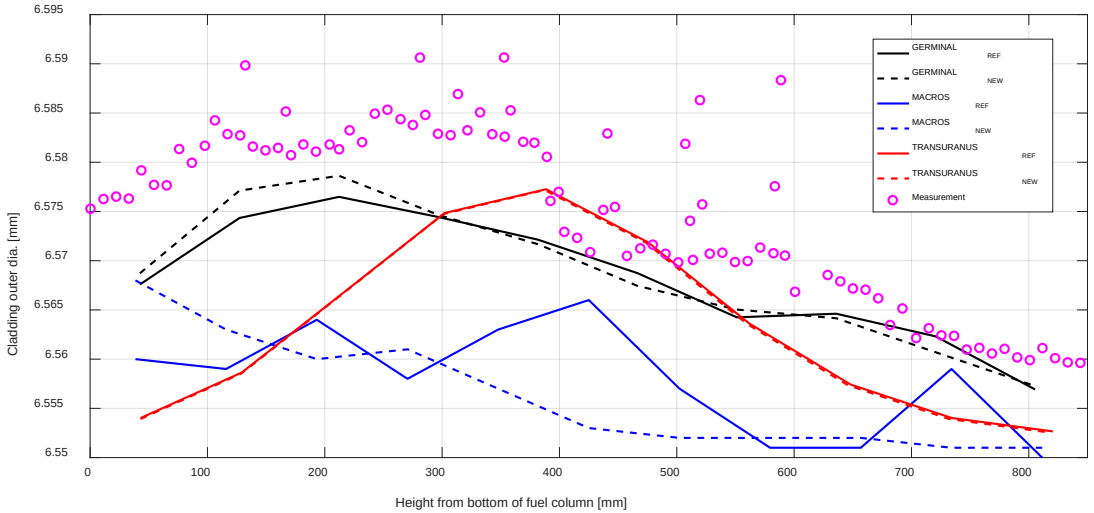

Figure 59. Axial profiles of the cladding outer diameter of the SUPERFACT-1 pin SF16 at end of life.

Table 8: Comparison between pre- and post-INSPYRE code results and experimental measurements [3] for fuel pin SF16 (X: not calculated).

	Measured	TU REF	TU THERMAL	TU MECHANICAL	TU SCIANTIX	TU NEW	GERMINAL REF	GERMINAL NEW	MACROS REF	MACROS NEW
Final burnup at ppn (at.%)	**6.4**	6.3	6.3	6.3	6.3	6.3	6.6	6.6	6.6	6.3
Fission gas (Xe + Kr) produced (cm^3)	**225***	226	226	223	289	229	227	227	236	224
Fission gas release (%)	**69**	47	48.4	55.8	6.8	7.6	53	68.5	54	60.9
Kr / (Kr + Xe) (%)	**6.9**	6.9	6.9	6.9	X	X	0.1	0.1	6.9	13.4
He released (cm^3)	**39.7**	28	28.8	27.4	X	X	61	60.9	38	25.0
Central hole length (mm)	**550 - 619**	777	691	777	775	518	425	425	541	618
Fuel elongation (mm)	**5.6 – 6.2**	25.5	25.8	23.7	19.7	20.3	0.5	0.4	39.1	16.9
Clad elongation (mm)	**1.5 – 2.3**	1.4	1.4	1.4	1.4	1.4	0.0	0.04	1.8	0.7

* Value calculated from experimental information.